Postprint of: Sabik A., Kreja I., Large thermo-elastic displacement and stability FEM analysis of multilayered plates and shells, Thin-Walled Structures, Vol. 71 (2013), pp. 119-133, DOI: 10.1016/j.tws.2013.05.002

Large thermo-elastic displacement and stability FEM analysis of multilayered plates and shells

Sabik A.*, Kreja I. **

Department of Structural Mechanics and Bridge Structures,
Gdansk University of Technology, Narutowicza 11/12, 80-233 Gdańsk, Poland

---

Abstract

The paper concerns the load capacity analysis of thermally loaded multilayered plates and shells. The multilayered body is treated as an equivalent single layer whose kinematics is consistent with the first-order shear deformation theory. The Authors focus on the thermo-elastic stability problem of the thin-walled structures. The equilibrium paths are traced with the use of Riks-Wempner-Ramm algorithm. By making use of the Tsai-Wu hypothesis the material's strength examination is included in the study. The considered problems are resolved with the Authors' program. The presented results confirm that proposed model can be very effective in the stability analysis of multilayered panels.

Keywords: temperature, multilayered shells, non-linear analysis, stability

*Corresponding author: agsa@pg.gda.pl

**Corresponding author: ikreja@pg.gda.pl

1.Introduction

Multilayered composite panels play nowadays an important role in many branches of industry. Wide applications of composites result from their attractive advantages like high strength-to-weight ratio, significant chemical and corrosion resistance or excellent thermal insulation parameters. Thus composite shells can work in a range of environments serving for example as fuselages of space vehicles, turbine blades in jet-engines, wind turbine blades,

chimney liners or industrial ducts. Consequently the structures can be subjected to various types of loadings, i.e. mechanical, chemical and thermal influences.

In this work the Authors concentrate on the load capacity of thermally influenced multilayered panels. It must be stressed, that the temperature impact can lead to many complex problems like [1]: instability or material degradation, e.g. reduction of strength and elastic properties, decrease of density [2], delamination [2, 3]; creep, thermal yielding, cracking etc.

This article is devoted to thermally induced instability of elastic panels. It is assumed, that the material properties remain constant during the loading process and the delamination mechanism does not occur, what is obviously - in view of above mentioned effects - a considerable simplification. However, by taking into account that the composite forming processes are still being improved, the assumption of a perfect bond can be partially justified. Secondly, one has to state, that most of composite panels are thin, slender constructions, which are able to withstand relatively high loads, particularly due to high strength of the materials themselves. As a result, the thin structures are usually highly susceptible to instability phenomenon, like buckling or snap-through, which can in such a situation occur before the strength of material is exceeded. Moreover, depending on slenderness, boundary conditions [4] but also a lamination-scheme [5-6], the regime of linear behavior of structure changes. Very often the geometrically non-linear effects arise before the instability takes place. Then, the most popular and simplest stability study method, namely linear eigenvalue problem analysis becomes insufficient. Therefore, the geometrically non-linear analysis seems to be a more appropriate attitude in this situation.

To the best of the Authors' knowledge, one of the most extensive surveys dedicated to temperature influence on composite structures and its analysis was published by Noor and Burton [3]. The authors of [3] reviewed many articles related to thermally induced instability

of composite panels, including about 80 works concerning bifurcation, although the majority of them are connected with plate problems. However, only 20 of the listed works deal with the non-linear analysis, and just 4 of them are associated with shells. Another essential work published in the early 90's is the article of Huang and Tauchert [5] concerning the geometrically non-linear analysis of multilayered plates and shells under a uniform temperature rise. Probably due to a significant number of numerical examples presented there, especially for shells, this work is still widely cited; see e.g. [7-14].

The valuable review [3] can be augmented by examining supplementary works published after 1992. The simplest analyses concerning the determination of critical temperatures obtained by means of linear eigenvalue problem are presented in [15-19]. In [20] the buckling temperature is determined from a closed formula resulting from the assumptions of classical thin plates theory, and the obtained solutions are compared with experimental data. Thermal buckling temperatures of plate strips supported along two opposite edges are analyzed in [21]. The author uses there the analogy to the bar theory to establish the formula for the thermal critical load of a transversely isotropic layer. In [22], on the other hand, the trigonometric series are employed to find the buckling temperatures.

The post-critical analysis is usually performed with the use of an incremental analysis taking into account large deformations. Mostly, the weak form of the boundary value problem and finite element method are utilized, see e. g. [5, 7, 9-12]. However, in [23-24] the post-critical paths are established on the basis of a sequential solution of the eigenvalue problem and in [25-26] to resolve the non-linear differential equations the Chebyshev series are adopted.

It is worth to mention that some authors consider thermo-mechanical influences [13, 19, 25-34]. Nevertheless, probably to avoid problems with a two-parametric load description, usually only one influence (i.e. mechanical load or temperature field) acts in such a case as an active load, while the second one remains constant during the analysis.

The degradation of material parameters caused by the temperature rise is analyzed in [13-14, 23, 25, 27, 35-37]. One has to stress, that the temperature-dependency functions are typically arbitral, like linear function [25, 35, 37] or higher-order polynomials [27]. A special piece-wise linear function is adopted in [13-14, 23, 36], whereas it must be noticed, that this approach is applied for one material only.

The stability study with simultaneous control of stress state in material is presented in [5, 13-14, 27]. In [5, 14] the failure initiation is detected by the use of Tsai-Wu hypothesis, while in [13] the Hashin criterion is employed. Another methodology is introduced in [27], where the value of bending energy is adopted as a failure control parameter. It is worth to state, that in all above mentioned cases the failure control has a passive character, i.e. the stiffness and strength parameters of material remain constant regardless of the failure progress.

In order to verify the sensitivity of the structure to certain conditions, the analysis of stability is usually extended by various parametric studies. The most distinctive parameters for the stability analysis of multilayered panels are: the influence of initial geometric imperfections [27, 32, 33, 37], boundary conditions [10-11, 13, 18-19, 23-24, 36, 38], lamination scheme [14, 18, 31, 33, 35-36, 39], and number of layers [5, 14, 33, 36]. One can find also more specific studies taking into account the influence of such factors as: the layout of stiffeners [9, 40], the size and orientation of a crack [15], the stochastic variability of material parameters [19], the moisture concentration [8], the location and size of a cut-out [7, 10, 31], or the temperature distribution in the thickness direction [7, 26, 39].

As stated earlier, the Authors of the present report focus on the thermo-elastic stability problem. The pre- and post-critical behavior of thermally loaded multilayered panels is investigated on the basis of the geometrically non-linear analysis within the Total Lagrangian description. The equilibrium paths are traced with the use of the Riks-Wempner-Ramm

algorithm. In each step the stress state is monitored according to the Tsai-Wu hypothesis; however, the material parameters are kept constant during the analysis.

In the incremental formulation presented below, the following notation has been adopted (cf. [41]): the left superscript describes the configuration in which the value is obtained, while the left subscript stands for the configuration the value refers to.

2. The shell description

The basic concept used in the present description of the shell is the Equivalent Single Layer (ESL) model, where it is assumed, that the multilayered medium can be described by the statically equivalent homogeneous single layer [42]. The ESL idea is one of the two-dimensional lamination theories [43] that consists in an appropriate reduction of a 3-D multi-layer medium into a 2-D single-layer body - an operation usually based on the pre- integration of the stress distribution in the cross-section during the computation of resultant forces. All variables are therefore connected with a reference surface (usually the middle surface) of the shell and their number is independent of the number of layers. As a consequence, the theories known for the homogeneous shells can be employed in the analysis of multilayered shells. Since composite materials are characterized by significant shear flexibility, the shell model should take into account the transverse shear deformation. To include this effect in two-dimensional formulations either the First-Order-Shear-Deformation (FOSD) or the Higher-Order-Shear-Deformation (HOSD) theories should be used. Although HOSD theories represent more advanced concept and therefore they can be more effective in the analysis of various problems, like for example thick panels [43]; their implementation requires a superior number of unknowns, what significantly limits the application of HOSD models in non-linear analyses [44]. The Authors of the present study recognize the FOSD concept as being

absolutely sufficient for the range of problems considered. The employed FOSD model of the shell is outlined in Appendix A.

2.1. *Thermal load distribution*

It is assumed, that the temperature distribution varies in a linear form in the thickness direction. Taking into account, that the shells considered in the paper are rather thin structures, this presumption seems to be fully justified. In order to provide a one-parameter load description in the incremental analysis, the ratio *p* between the maximum temperatures at the top and bottom surfaces remains constant during the loading process. The general formula describing the temperature distribution has the following form:

$$
\begin{aligned}
&{}^{m}_{0}T(\theta^3) = T^{(0)} + T^{(1)}\theta^3, \\
&T^{(0)} = {}^{m}\lambda_{th} \cdot T_{max}\left(\frac{1+p}{2}\right) - {}^{m}\lambda_{th} \cdot T_{init}, \\
&T^{(1)} = SIGN \cdot {}^{m}\lambda_{th} \cdot T_{max}\left(\frac{1-p}{H}\right),
\end{aligned}
\tag{1}
$$

where ${}^{m}\lambda_{th}$ is the load parameter; T_{init} stands for the initial temperature, which is assumed to be the same on the opposite external surfaces; T_{max} is a presumed maximum value of so called leading temperature, i.e. on the chosen external surface. *H* is the thickness of the shell, *p* is the ratio between maximum temperature values on the outer surfaces and *SIGN* is a supporting two-value parameter:

$$
\begin{aligned}
&SIGN = 1 \quad \Leftrightarrow \quad p = \frac{T_{b,max}}{T_{t,max}}, \\
&SIGN = -1 \quad \Leftrightarrow \quad p = \frac{T_{t,max}}{T_{b,max}}.
\end{aligned}
\tag{2}
$$

$T_{t,max}$ and $T_{b,max}$ are presumed maximum temperature values on top and bottom surface of the shell, respectively. The temperature in denominators in (2) is a leading one.

One can observe that for *p*=1 the formula (1) describes the uniform temperature distribution.

2.2. *Constitutive law of a single layer*

The layers of laminated structures are usually made of isotropic or transversely isotropic materials. Figure 1 presents the orientation of the local material axes *a*-*b*-*c*. The angle α_k is a measure of the deviation of the longitudinal direction (*a*) of a layer from the global axis θ^1. The following stress-strain relations correspond to the general case of a monoclinic medium.

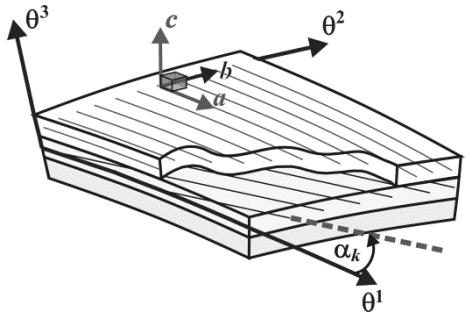

Fig. 1. Local axes of transversely isotropic material

Due to the thermo-mechanical coupling, the elastic strains are dependent on the thermal strains, so the effective stresses are given as follows

$$\left\{{}^{m}S_{ef}\right\} = \left[\mathrm{C}_{m}\right]\left(\left\{{}^{m}E\right\} - \left\{{}^{m}E^{th}\right\}\right) \quad \Leftrightarrow \quad \left\{{}^{m}S_{ef}\right\} = \left\{{}^{m}S_{mech}\right\} - \left\{{}^{m}S_{th}\right\}, \tag{3}$$

where $\left\{{}^{m}E\right\}$, $\left\{{}^{m}E^{th}\right\}$ are displacement dependent and thermal strain vectors, $\left\{{}^{m}S_{mech}\right\}$, $\left\{{}^{m}S_{th}\right\}$, $\left\{{}^{m}S_{ef}\right\}$ are mechanical, thermal and effective stress vectors, respectively, and $\left[\mathrm{C}_{m}\right]$ is the constitutive matrix.

In an incremental formulation of nonlinear problems the mechanical strains and stresses must be decomposed into a sum of the actual value and the increment [41]. The constitutive relations must be then given in an incremental form, which in local material axes can be expressed as follows

$$\begin{Bmatrix} {}_{0}S_{mech}^{aa} \\ {}_{0}S_{mech}^{bb} \\ {}_{0}S_{mech}^{ab} \\ {}_{0}S_{mech}^{bc} \\ {}_{0}S_{mech}^{ac} \end{Bmatrix} = \left[\mathrm{C}_{m}\right] \begin{Bmatrix} {}_{0}E_{aa} \\ {}_{0}E_{bb} \\ 2\,{}_{0}E_{ab} \\ 2\,{}_{0}E_{bc} \\ 2\,{}_{0}E_{ac} \end{Bmatrix}. \tag{4}$$

On the other hand, the thermal strains and stresses are displacement independent and therefore they do not need to be decomposed. As a result, one gets the constitutive relations expressed in the material axes *a*-*b*-*c* as:

$$\begin{Bmatrix} {}^{m}_{0}S^{aa}_{th} \\ {}^{m}_{0}S^{bb}_{th} \\ 0 \\ 0 \\ 0 \end{Bmatrix} = [\mathrm{C}_m] \begin{Bmatrix} {}^{m}_{0}E^{th}_{aa} \\ {}^{m}_{0}E^{th}_{bb} \\ 0 \\ 0 \\ 0 \end{Bmatrix} = [\mathrm{C}_m] \begin{Bmatrix} \alpha^{th}_{aa} \\ \alpha^{th}_{bb} \\ 0 \\ 0 \\ 0 \end{Bmatrix} {}^{m}_{0}T(\theta^3), \tag{5}$$

where α^{th}_{aa}, α^{th}_{bb} are the thermal expansion coefficients in directions of the axes *a* and *b*, respectively, (Figure 1) and ${}^{m}_{0}T(\theta^3)$ is the temperature at the considered point in the configuration *t*=*m*.

The components of the local material matrix $[\mathrm{C}_m]$ are following:

$$[\mathrm{C}_m] = \begin{bmatrix} \frac{E_a}{1-\nu_{ab}\nu_{ba}} & \frac{\nu_{ab}E_b}{1-\nu_{ab}\nu_{ba}} & 0 & 0 & 0 \\ \frac{\nu_{ba}E_a}{1-\nu_{ab}\nu_{ba}} & \frac{E_b}{1-\nu_{ab}\nu_{ba}} & 0 & 0 & 0 \\ 0 & 0 & G_{ab} & 0 & 0 \\ 0 & 0 & 0 & (k)G_{bc} & 0 \\ 0 & 0 & 0 & 0 & (k)G_{ab} \end{bmatrix}, \tag{6}$$

where E_a and E_b are the Young's moduli in the directions of the axes *a* and *b*, respectively, G_{ab}, G_{bc}, G_{ac} are the shear moduli in the planes *a*-*b*, *b*-*c*, *a*-*c*, respectively, and ν_{ab} is the Poisson's ratio in the plane *a*-*b*. For the orthotropic material [45] the following relation is in force

$$E_a\nu_{ba} = E_b\nu_{ab}\,. \tag{7}$$

The *k* parameter in (6) stands for the shear correction factor. It is introduced to compensate the overestimated transverse shear strain energy which follows from the constant distribution of these strains in the FOSD concept, see (A.10). The determination of the *k* value in multilayered media is still an open question [46]. Very often it is set to 5/6, according to Reissner. Nevertheless, in (6) *k* is given in parentheses, because in the present work the shear

factors are not introduced at the layer level; instead, they are evaluated numerically for the whole cross-section and for each transverse shear plane, see (B.13). The adopted procedure is well known in the literature [47-48] - a value of the composite transverse shear correction factor is determined by matching the transverse shear strain energy predicted by the FOSD model with that obtained from the three-dimensional elasticity theory. As shown in [12, 46] such an approach combines a simplicity with a significant effectiveness.

The above stress-strain relations are given in the local material axes, but for practical application they need to be transformed into the global coordinate system θ^1-θ^2-θ^3 (Figure 1). The following transformation rules are valid

$$\left\{\begin{array}{c} {}_0S^{11}_{mech} \\ {}_0S^{22}_{mech} \\ {}_0S^{12}_{mech} \\ {}_0S^{23}_{mech} \\ {}_0S^{13}_{mech} \end{array}\right\} = [\mathrm{T}]^T \left\{\begin{array}{c} {}_0S^{aa}_{mech} \\ {}_0S^{bb}_{mech} \\ {}_0S^{ab}_{mech} \\ {}_0S^{bc}_{mech} \\ {}_0S^{ac}_{mech} \end{array}\right\}, \quad \left\{\begin{array}{c} {}_0E_{aa} \\ {}_0E_{bb} \\ 2\,{}_0E_{ab} \\ 2\,{}_0E_{bc} \\ 2\,{}_0E_{ac} \end{array}\right\} = [\mathrm{T}] \left\{\begin{array}{c} {}_0E_{11} \\ {}_0E_{22} \\ 2\,{}_0E_{12} \\ 2\,{}_0E_{23} \\ 2\,{}_0E_{13} \end{array}\right\}, \quad \left\{\begin{array}{c} {}^m_0S^{11}_{th} \\ {}^m_0S^{22}_{th} \\ {}^m_0S^{12}_{th} \\ 0 \\ 0 \end{array}\right\} = [\mathrm{T}]^T \left\{\begin{array}{c} {}^m_0S^{aa}_{th} \\ {}^m_0S^{bb}_{th} \\ 0 \\ 0 \\ 0 \end{array}\right\}, \tag{8}$$

with the transformation matrix:

$$[\mathrm{T}] = \begin{bmatrix} \cos^2(\alpha_k) & \sin^2(\alpha_k) & \frac{1}{2}\sin(2\alpha_k) & 0 & 0 \\ \sin^2(\alpha_k) & \cos^2(\alpha_k) & -\frac{1}{2}\sin(2\alpha_k) & 0 & 0 \\ -\sin(2\alpha_k) & \sin(2\alpha_k) & \cos(2\alpha_k) & 0 & 0 \\ 0 & 0 & 0 & \cos(\alpha_k) & -\sin(\alpha_k) \\ 0 & 0 & 0 & \sin(\alpha_k) & \cos(\alpha_k) \end{bmatrix}. \tag{9}$$

One can observe, that after the transformation, the third thermal stress component occurs in the global coordinate system θ^1-θ^2-θ^3 (8). Finally we get the stress-strain relations in global axes:

$$\begin{Bmatrix} {}_0S^{11}_{mech} \\ {}_0S^{22}_{mech} \\ {}_0S^{12}_{mech} \\ {}_0S^{23}_{mech} \\ {}_0S^{13}_{mech} \end{Bmatrix} = [\mathrm{T}]^T [\mathrm{C}_m][\mathrm{T}] \begin{Bmatrix} {}_0E_{11} \\ {}_0E_{22} \\ 2\,{}_0E_{12} \\ 2\,{}_0E_{23} \\ 2\,{}_0E_{13} \end{Bmatrix} \quad \Leftrightarrow \quad \begin{Bmatrix} {}_0S^{11}_{mech} \\ {}_0S^{22}_{mech} \\ {}_0S^{12}_{mech} \\ {}_0S^{23}_{mech} \\ {}_0S^{13}_{mech} \end{Bmatrix} = [\mathrm{C}] \begin{Bmatrix} {}_0E_{11} \\ {}_0E_{22} \\ 2\,{}_0E_{12} \\ 2\,{}_0E_{23} \\ 2\,{}_0E_{13} \end{Bmatrix},$$

$$\begin{Bmatrix} {}^m_0S^{11}_{th} \\ {}^m_0S^{22}_{th} \\ {}^m_0S^{12}_{th} \\ 0 \\ 0 \end{Bmatrix} = [\mathrm{T}]^T [\mathrm{C}_m] \begin{Bmatrix} \alpha^{th}_{aa} \\ \alpha^{th}_{bb} \\ 0 \\ 0 \\ 0 \end{Bmatrix} {}^m_0T(\theta^3) \quad \Leftrightarrow \quad \begin{Bmatrix} {}^m_0S^{11}_{th} \\ {}^m_0S^{22}_{th} \\ {}^m_0S^{12}_{th} \\ 0 \\ 0 \end{Bmatrix} = \{\mathrm{C}_{th}\} \, {}^m_0T(\theta^3). \tag{10}$$

The corresponding constitutive relations valid at the cross-section level can be found in Appendix B.

3.Incremental analysis

In order to distinguish configurations in Total Lagrangian description, the following convention regarding the left superscript is adopted: the reference configuration is the initial one (t=0), the actual configuration refers to t=1 and the unknown one corresponds to t=2. The appropriate incremental decomposition of the virtual work principle is presented in Appendix B, whereas the derivation of the incremental equilibrium equation is described in Appendix C.

In the incremental analysis the load is usually defined as a reference load multiplied by a load factor. In the case of thermal influences within the framework of Total Lagrangian description the load vector is dependent on the actual displacements (C.6), therefore, the attention should be paid to an implementation of an appropriate expression for the incremental load. The formula ${}^2_0\mathbf{F}_{th} = {}^2\lambda_{th}\,\mathbf{F}_{th,REF}$ would be rather inadequate, because in this case a constant reference vector $\mathbf{F}_{th,REF}$ does not exist. In point of fact, the reference term is constituted by the leading temperature amplitude

$$\Delta T_{REF} = T_{max} - T_{init}\,, \tag{11}$$

at the chosen shell surface (see (1)).

The thermal load vector ${}^{2}_{0}\mathbf{F}_{th}$ and thermal stiffness matrix ${}^{2}_{0}\mathbf{K}_{G,th}$ will be then expressed as

$$\begin{aligned} {}^{2}_{0}\mathbf{F}_{th} &= {}^{2}\lambda_{th}\,\mathbf{F}_{th}\left({}^{1}\mathbf{q},\Delta T_{REF}\right), \\ {}^{2}_{0}\mathbf{K}_{G,th} &= {}^{2}\lambda_{th}\,\mathbf{K}_{G,th}\left(\Delta T_{REF}\right), \end{aligned} \tag{12}$$

and the incremental equation (C.13) can be then rewritten into

$$\left({}^{1}_{0}\mathbf{K}_{U}+{}^{1}_{0}\mathbf{K}_{G}-{}^{2}\lambda_{th}\mathbf{K}_{G,th}\left(\Delta T_{REF}\right)\right)\Delta\mathbf{q}={}^{2}\lambda_{th}\mathbf{F}_{th}\left({}^{1}\mathbf{q},\Delta T_{REF}\right)-{}^{1}_{0}\mathbf{F}\,, \tag{13}$$

where ${}^{1}_{0}\mathbf{K}_{U}$, ${}^{1}_{0}\mathbf{K}_{G}$, $\mathbf{K}_{G,th}$ are the particular parts of the global stiffness matrix (cf. (C.7-C.9)), $\mathbf{F}_{th}$ and ${}^{1}_{0}\mathbf{F}$ are the thermal load vector and balanced force vector (cf. (C.6) and (C.5)).

In (13) it is emphasized, that the thermal load vector depends on the actual displacements. It is also worth to mention that the thermal stiffness matrix depends on the unknown temperature value. To simplify the notation a shorter version of (13) is introduced:

$$\mathbf{K}\left({}^{1}\mathbf{q},{}^{2}\lambda_{th},\Delta T_{REF}\right)\Delta\mathbf{q}={}^{2}\lambda_{th}\mathbf{F}_{th}\left({}^{1}\mathbf{q},\Delta T_{REF}\right)-\mathbf{F}\left({}^{1}\mathbf{q}\right). \tag{14}$$

3.1. *Riks-Wempner-Ramm algorithm*

To trace the equilibrium path of the structure the arc-length method is implemented, or more specifically, the Riks-Wempner-Ramm (RWR) algorithm [49]. In order to distinguish the increment and iteration numbers two superscripts are employed: the left one stands for the increment (step) number (*n*), while the right one refers to the number of the iteration (*i*). Each step (*n*) of the analysis starts with the calculation of the zero approximation of the displacement and load parameter increments which are combined by the mix parameter – arc-length (*ds*) - as follows:

$$\left({}^{n}\Delta\mathbf{q}^{(0)}\right)^{T}\left({}^{n}\Delta\mathbf{q}^{(0)}\right)+\left({}^{n}\Delta\lambda_{th}^{(0)}\right)^{2}={}^{n}ds^{2} \tag{15}$$

The zero approximation of the displacement increment depends on the load parameter and the reference displacement increments

$${}^{n}\Delta\mathbf{q}^{(0)}={}^{n}\Delta\lambda_{th}^{(0)}\,{}^{n}\Delta\mathbf{q}_{REF}\,, \tag{16}$$

where $\Delta\mathbf{q}_{REF}$ results from the solution of the following equation:

$$\mathbf{K}\left({}^{(n-1)}\mathbf{q},\,{}^{(n-1)}\lambda_{th},\Delta T_{REF}\right){}^{n}\Delta\mathbf{q}_{REF}=\mathbf{F}_{th}\left({}^{(n-1)}\mathbf{q},\Delta T_{REF}\right). \tag{17}$$

One has to notice, that on the right side of (17) only the temperature amplitude is present, while on the left side the stiffness matrix is built in the accordance with the actual temperature value.

By substituting (16) into (15) we get

$$\left({}^{n}\Delta\lambda_{th}^{(0)}\right)^{2}\left[\left({}^{n}\Delta\mathbf{q}_{REF}\right)^{T}\left({}^{n}\Delta\mathbf{q}_{REF}\right)+1\right]={}^{n}ds^{2}. \tag{18}$$

As the arc-length parameter is known, the relation (18) enables to find the unknown value of the load parameter. However, in the first step (n=1) of the analysis the load parameter increment is predefined and the arc-length value is obtained from (18). On the other hand, in next steps the arc-length value is scaled according to convergence condition

$${}^{n}ds^{2}=\sqrt{\frac{NDIT}{NITE}}\,{}^{(n-1)}ds^{2},\qquad n>1, \tag{19}$$

where *NDIT* and *NITE* are the numbers of iterations performed in the previous step and the desired number of iterations, respectively.

Moreover, the arc-length parameter should satisfy an additional condition

$$ds_{min}<{}^{n}ds<ds_{max}, \tag{20}$$

where ds_{min} and ds_{max} are the prescribed minimum and maximum values.

Finally the zero approximation of the displacement vector and the load parameter can be found from the relations:

$$\begin{aligned}{}^{n}\mathbf{q}^{(0)}&={}^{(n-1)}\mathbf{q}+{}^{n}\Delta\mathbf{q}^{(0)},\\ {}^{n}\lambda_{th}^{(0)}&={}^{(n-1)}\lambda_{th}+{}^{n}\Delta\lambda_{th}^{(0)}.\end{aligned} \tag{21}$$

The next approximation of the displacement vector and the load parameter can be estimated as

$$\begin{aligned}{}^{n}\mathbf{q}^{(i)}&={}^{n}\mathbf{q}^{(i-1)}+{}^{n}\delta\mathbf{q}^{(i)},\\ {}^{n}\lambda_{th}^{(i)}&={}^{n}\lambda_{th}^{(i-1)}+{}^{n}\delta\lambda_{th}^{(i)},\end{aligned} \tag{22}$$

where ${}^{n}\delta\mathbf{q}^{(i)}$ and ${}^{n}\delta\lambda_{th}^{(i)}$ are the corrections obtained in the iteration process.

The incremental equation (14) which is to be resolved during the iterations can be rewritten as follows:

$$\mathbf{K}\left({}^{n}\mathbf{q}^{(i-1)},\,{}^{n}\lambda_{th}^{(i-1)},\Delta T_{REF}\right){}^{n}\delta\mathbf{q}^{(i)} = {}^{n}\delta\lambda_{th}^{(i)}\mathbf{F}_{th}\left({}^{n}\mathbf{q}^{(i-1)},\Delta T_{REF}\right)+\mathbf{J}_{U}\left({}^{n}\mathbf{q}^{(i-1)},\Delta T_{REF}\right), \tag{23}$$

where

$$\mathbf{J}_{U}\left({}^{n}\mathbf{q}^{(i-1)},\Delta T_{REF}\right) = {}^{n}\lambda_{th}^{(i-1)}\mathbf{F}_{th}\left({}^{n}\mathbf{q}^{(i-1)},\Delta T_{REF}\right)-\mathbf{F}\left({}^{n}\mathbf{q}^{(i-1)}\right) \tag{24}$$

is an unbalanced force vector (cf. (C.12)). It must be stressed, that on the right side of (23) the unknown temperature value is present, whereas the stiffness matrix is obtained with the use of the actual temperature.

The calculated zero approximations of displacement and load parameter increments are the components of the tangent vector:

$${}^{n}\mathbf{t}^{(0)} = \left[\,{}^{n}\Delta\mathbf{q}^{(0)},\,{}^{n}\Delta\lambda_{th}^{(0)}\,\right], \tag{25}$$

while the unknown corrections compose the vector

$${}^{n}\delta\Delta^{(i)} = \left[\,{}^{n}\delta\mathbf{q}^{(i)},\,{}^{n}\delta\lambda_{th}^{(i)}\,\right]. \tag{26}$$

In the subsequent iterations the tangent vector (25) is updated and composed as:

$${}^{n}\mathbf{t}^{(i-1)} = \left[\,{}^{n}\Delta\mathbf{q}^{(i-1)},\,{}^{n}\Delta\lambda_{th}^{(i-1)}\,\right]. \tag{27}$$

The RWR algorithm states, that in each iteration the vector ${}^{n}\delta\Delta^{(i)}$ is perpendicular to the vector ${}^{n}\mathbf{t}^{(i-1)}$, thus

$${}^{n}\mathbf{t}^{(i-1)}\cdot{}^{n}\delta\Delta^{(i)} = 0\,. \tag{28}$$

By substituting (26) and (27) into (28) one get the expression

$$\left({}^{n}\Delta\mathbf{q}^{(i-1)}\right)^{T}\left({}^{n}\delta\mathbf{q}^{(i)}\right)+{}^{n}\Delta\lambda_{th}^{(i-1)}\,{}^{n}\delta\lambda_{th}^{(i)} = 0\,. \tag{29}$$

The displacement correction is decomposed in the following form

$${}^{n}\delta\mathbf{q}^{(i)} = {}^{n}\delta\lambda_{th}^{(i)}\,{}^{n}\delta\mathbf{q}_{F}^{(i)} + {}^{n}\delta\mathbf{q}_{J}^{(i)}, \tag{30}$$

which corresponds to the decomposition of the equation (23):

$$\begin{aligned}\mathbf{K}\left({}^{n}\mathbf{q}^{(i-1)},\,{}^{n}\lambda_{th}^{(i-1)},\Delta T_{REF}\right){}^{n}\delta\mathbf{q}_{F}^{(i)}&=\mathbf{F}_{th}\left({}^{n}\mathbf{q}^{(i-1)},\Delta T_{REF}\right),\\ \mathbf{K}\left({}^{n}\mathbf{q}^{(i-1)},\,{}^{n}\lambda_{th}^{(i-1)},\Delta T_{REF}\right){}^{n}\delta\mathbf{q}_{J}^{(i)}&=\mathbf{J}_{U}\left({}^{n}\mathbf{q}^{(i-1)},\Delta T_{REF}\right).\end{aligned} \tag{31}$$

Moreover, by introducing (30) to (29) one gets the following expression

$${}^{n}\delta\lambda_{th}^{(i)}=\frac{-\left({}^{n}\Delta\mathbf{q}^{(i-1)}\right)^{T}\left({}^{n}\delta\mathbf{q}_{J}^{(i)}\right)}{\left({}^{n}\Delta\mathbf{q}^{(i-1)}\right)^{T}\left({}^{n}\delta\mathbf{q}_{F}^{(i)}\right)+{}^{n}\Delta\lambda_{th}^{(i-1)}}. \tag{32}$$

Finally the solutions of (31), together with (32) and (30) enable to find the required corrections in the subsequent iterations and correct the result (21) according to (22).

The main advantage of the arc-length technique is the ability to trace the unstable parts of equilibrium paths. However, in order to distinguish whether the load increment ${}^{n}\Delta\lambda_{th}^{(0)}$ (18) should increase or decrease an appropriate unloading condition is required. Very often, a criterion basing on the sign of the global stiffness matrix is adopted, i.e.:

$$\operatorname{sgn}\left({}^{n}\Delta\lambda_{th}^{(0)}\right)=\operatorname{sgn}\left|\mathbf{K}\left({}^{(n-1)}\mathbf{q},\,{}^{(n-1)}\lambda_{th},\Delta T_{REF}\right)\right|. \tag{33}$$

The condition (33) works well at the load limit points but it fails at the bifurcation points by leading to characteristic oscillatory problems. Since the junction points are very characteristic for thermally induced shells, this criterion is usually insufficient in that kind of the analysis. Therefore, in the present study the condition suggested in [50] has been implemented as an alternative, which states, that:

$$\left({}^{(n-1)}\Delta\right)^{T}\cdot\left({}^{n}\mathbf{t}^{(0)}\right)>0, \tag{34}$$

where ${}^{(n-1)}\Delta$ is the vector composed of the displacement and load parameter increments obtained in the previous step:

$${}^{(n-1)}\Delta=\left[{}^{(n-1)}\Delta\mathbf{q},\,{}^{(n-1)}\Delta\lambda_{th}\right]. \tag{35}$$

From (34), by the use of (16), we get

$${}^{n}\Delta\lambda_{th}^{(0)}\left(\left({}^{(n-1)}\Delta\mathbf{q}\right)^{T}\left({}^{n}\Delta\mathbf{q}_{REF}\right)+{}^{(n-1)}\Delta\lambda_{th}\right)>0, \tag{36}$$

which means, that

$$\operatorname{sgn}\left({}^{n}\Delta\lambda_{th}^{(0)}\right)=\operatorname{sgn}\left(\left({}^{(n-1)}\Delta\mathbf{q}\right)^{T}\left({}^{n}\Delta\mathbf{q}_{REF}\right)+{}^{(n-1)}\Delta\lambda_{th}\right). \tag{37}$$

The criterion (37) allows to overcome the bifurcation points and to trace the path in the direction determined in the previous step.

4.Numerical examples

As the examination of the proposed numerical model some illustrative examples are presented. All of them are resolved with the use of the Authors' own program in which 8-node Serendipity and 9– and 16-node Lagrange finite elements are available [51]. The analysis of the elements efficiency is widely discussed in [51]. Basing on that, in the present study the doubly curved 8-node Serendipity element with uniform reduced integration technique (8URI) is routinely used. To control the unloading criteria in the RWR algorithm, the steering parameter ICRIT is introduced. Its value is set to 0, which corresponds to condition (33) or 1, which refers to criterion (37). If not specified, the condition (37) (ICRIT=1) is employed.

In each incremental step the stress state in material is controlled according to the Tsai-Wu hypothesis [44, 45]. The failure control is performed at the Gauss points located in the middle of the thickness of each layer in every finite element. The failure mechanism is recognized in an approximate manner, i.e. depending on the part, which dominates in Tsai-Wu polynomial.

4.1. *Multilayered plate subjected to thermal gradient*

This example was proposed in [7]. A square plate (A=B=254mm) subjected to the thermal gradient is analyzed (Figure 2).

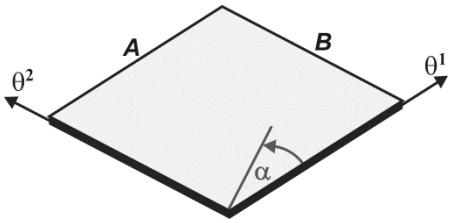

Fig. 2. Geometry of square plate

The panel is made of 16 layers of the thickness H_L=0.127mm each, with fibers oriented according to the scheme $[45^o/-45^o/0^o/90^o]_{2s}$. Every one layer is composed of the same material with properties: E_a=130.3GPa, E_b=9.37GPa, $G_{ab}=G_{ac}=G_{bc}$=4.5GPa, v_{ab}=0.33, $\alpha_{aa}^{th}=0.139\cdot10^{-6}1/^oC$, $\alpha_{bb}^{th}=9\cdot10^{-6}1/^oC$. The plate is simply supported with two opposite edges immovable in three directions, whereas the other edges are free to translate in in-plane directions. Additionally, in order to preserve the boundaries from wrinkling, the rotations about the normal lines to the edges are fixed. The mesh of 10x10 8URI elements is used in the study. The thermal gradient is described by the parameter $p=T_t/T_b$, where T_t and T_b are the maximum temperature values on the top and bottom surface of the plate. In the original study [7] following gradients p=0, 0.3, 0.6, 0.8, 0.9, 0.95 and their reciprocal are considered. The present analysis is extended by the examination of the uniform heating (p=1) and p=0.999 and p=1/0.999. The two latter cases can be treated as numerical approximations of the uniform temperature rise.

Figure 3 presents the normalized deflection of the central point in relation to the temperature on the middle surface of the plate. The reference results are marked with broken lines. One can observe that the present solutions match very well the reference ones. The additional studies of the influence of gradients p=0.999 and p=1/0.999 suggest, that the uniformly heated plate has a bifurcation point about 220ºC. This fact is supported by the results obtained for p=1 with ICRIT=0. Employing of the condition (33) results in oscillatory problems at 220ºC. It can be seen that for ICRIT=1 the bifurcation point is surpassed without any problems. However, the path above the junction point is obviously unstable.

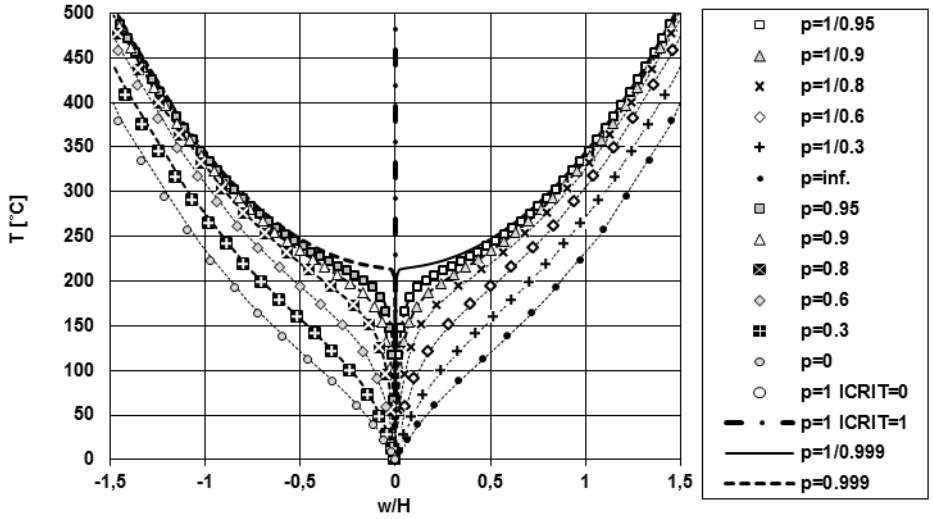

Fig. 3. The deflection of the central point of the plate subjected to the thermal gradients

4.2. *Multilayered plate under uniform thermal loading*

Following the proposal from [14] a square plate of the ratio A/H=100 (Figure 2) under a uniform temperature rise is analyzed. All four edges of the plate are fixed against the three translations and rotations about the normal lines to the edges. The laminate is made of 16 layers of the same material with following parameters: E_a=141GPa, E_b=13.1GPa, $G_{ab}=G_{ac}=G_{bc}$=9.31GPa, ν_{ab}=0.28, $\alpha_{aa}^{th}=0.18\cdot10^{-6}$1/ºC, $\alpha_{bb}^{th}=21.8\cdot10^{-6}$1/ºC, $X_t=X_c$=1650MPa, Y_t=58.9MPa, Y_c=236MPa, S_s=106MPa. Three lamination schemes are considered: cross-ply $[0º/90º]_{4s}$, quasi-isotropic $[45º/-45º/0º/90º]_{2s}$ and angle-ply $[45º/-45º]_{4s}$. The initial temperature is T_{init}=20ºC. The whole plate is discretized with 8x8 8URI elements. Due to the symmetry of the lamination schemes the bifurcation points can be expected in the equilibrium path, similarly as in the example 4.1. To avoid the oscillatory problems the uniform temperature rise is approximated with small thermal gradient T_d/T_g=0.9999. It is worth to notice, that in [14], to reach this objective, small perturbation forces were applied to the structure.

The agreement of present results with the reference solutions is demonstrated in Figure 4, where the reference ones are marked with broken lines. The small discrepancies observed in the post-buckling range can be explained by reading errors during reconstruction of results

from the graphs published in [14]. The results show, that the buckling temperature depends on the lay-up. The critical temperatures are T_{cr}=63ºC (64ºC), T_{cr}=81ºC (81ºC), T_{cr}=87ºC (81ºC) in the case of cross-ply, quasi-isotropic and angle-ply schemes, respectively, while in parentheses the reference results are given. The critical temperature of the angle-ply plate reported in [14] as being equal to 81ºC seems to be mistaken (compare Figure 4).

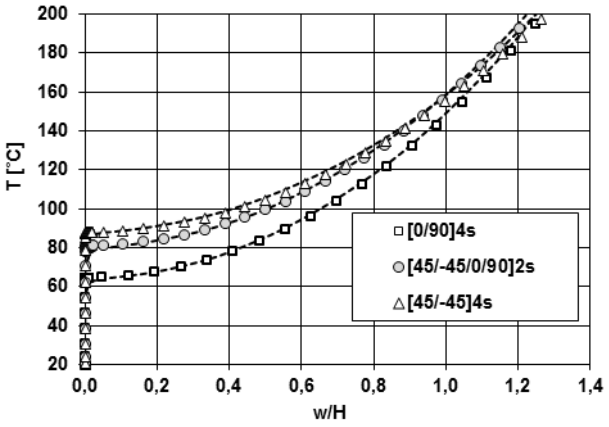

Fig. 4. The deflection of the central point of the plates subjected to the uniform heating

In this example the strength analysis was performed leading to the conclusion, that the failure occurs at temperature levels T_{TW}=810ºC (794.5 ºC), T_{TW}=738ºC (700ºC), T_{TW}=712ºC (691ºC) for, respectively, cross-ply, quasi-isotropic and angle-ply plate. The present results are comparable with the reference ones given in parentheses. According to the examination of dominating parts in the Tsai-Wu polynomial (38) the material fails due to the matrix cracking in outer layers.

Moreover, it can be observed, that the cross-ply scheme preserves the highest strength with the lowest buckling resistance.

It must be however stressed, that the failure temperatures reported above are very high and rather unrealistic, what is a consequence of neglecting the thermal degradation of material properties during computations. Nevertheless, one can observe, that the material strength is exceeded after the loss of stability takes place.

4.3. *Orthotropic cylindrical shell under uniform thermal loading*

This example was proposed in [5] and analyzed among others in [7, 9-10]. A behavior of a cylindrical orthotropic shell under uniform temperature rise is examined. The geometric data are: $A=B=R\phi$, R/A=5, A/H=200 (Figure 5). All the edges are fixed against the translations in three directions and rotations about the normal lines to the edges. The shell consists of one layer with reinforcement oriented in the circumferential direction and is made of the material with following properties: E_a=138GPa, E_b=8.28GPa, $G_{ab}=G_{ac}=G_{bc}$=6.9GPa, v_{ab}=0.33, $\alpha_{aa}^{th}=0.18\cdot10^{-6}$1/°C, $\alpha_{bb}^{th}=27\cdot10^{-6}$1/°C, $X_t=X_c$=1263MPa, Y_t=33.7MPa, Y_c=207MPa, S_s=57.3MPa.

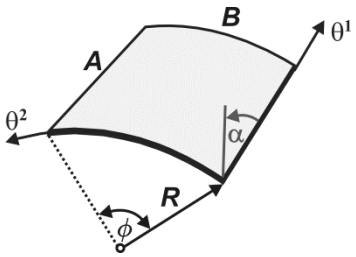

Fig. 5. Geometry of cylindrical shell

In papers [5, 7, 10] and probably also in [9] the symmetry conditions were adopted and a quarter of the structure was analyzed. By taking into account, that such an approach eliminates the possibility of unsymmetrical deformations, in the present study the whole shell is examined with mesh density of 16x16 8URI elements.

Figure 6 presents the equilibrium path of the normalized deflection of the central point. The solution obtained with the use of condition ICRIT=1 matches very well the reference path of Huang [5]. In 84ºC the shell loses the stability due to the snap-through phenomenon.

On the other hand, the application of the criterion ICRIT=0 leads to the oscillatory problems at about 80ºC and only a part of the path can be found. This fact implies the possibility of bifurcation point's presence at this temperature level. It has to be noticed, that in an additional study with the usage of symmetry conditions and criterion ICRIT=0, the convergence problems do not occur.

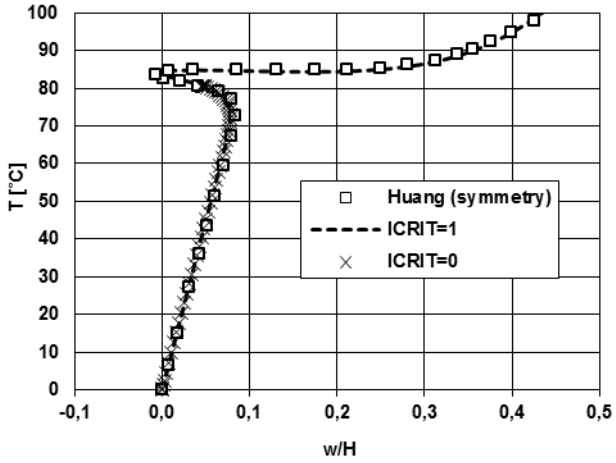

Fig. 6. Central deflection of the perfect cylindrical shell

In order to trace the possible secondary path the supplementary computations were performed with small transverse perturbation forces, which were removed from the model after the quality change of the path was detected. The location of the imperfections was not obvious and therefore it was determined by a trial and error method. Figure 7 illustrates the points the perturbations forces were applied at.

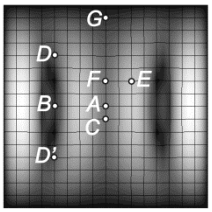

Fig. 7. Locations of perturbation forces

The imperfections situated on the longitudinal symmetry axis, i.e. at the points A and B did not change the solution obtained for the perfect case. However, the application of forces at the points D and E (also D') leads to the result shown in Figure 8. The junction point arises, as expected, at about 80ºC. The perturbations forces required to cause the path change in this case were very small – their magnitude was estimated at the level that in linear analysis produced the transverse deflection equal to 0.001*H*.

The perturbation forces of the above mentioned intensity at the points C and F were insufficient to modify the result shown in Figure 6. Nonetheless, after increasing the

perturbation forces to the level corresponding to the linear transverse deflections of 0.01*H*, the alternative result as shown in Figure 9 was obtained. In this case the bifurcation point refers to the temperature 82ºC.

Figure 10 demonstrates the deformations of the shell in 100ºC corresponding to three equilibrium paths. One can observe that the shape modes connected with the secondary paths are not bisymmetrical. It is also worth to stress that the detected deformation changes corresponding to both bifurcation points have a dynamic nature what is manifested through the characteristic decrease of load values after the paths' changes and the occurrence of turning points (Fig. 8-9). Both bifurcation points are then unstable.

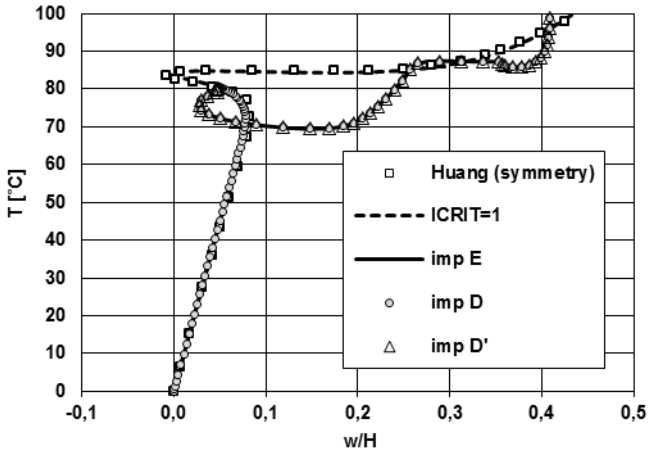

Fig. 8. Cylindrical shell. Comparison of fundamental and secondary path (imperfections at points D, D', E)

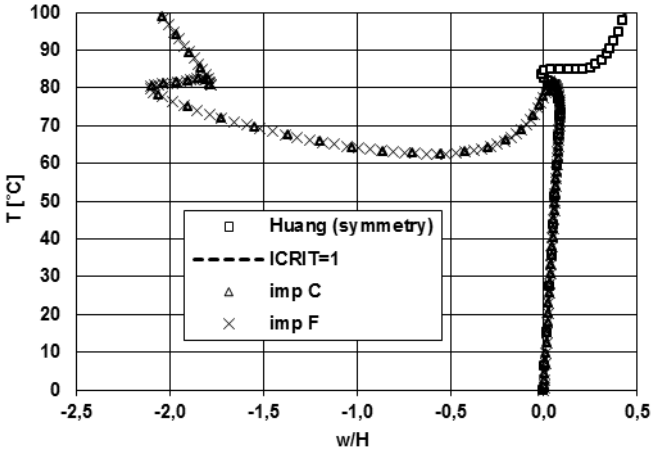

Fig. 9. Cylindrical shell. Comparison of fundamental and secondary path (imperfections at points C, F)

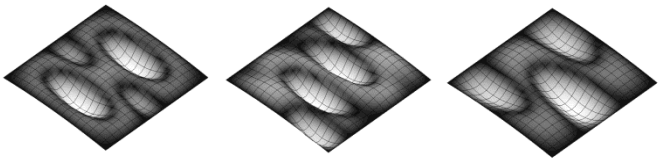

Fig. 10. Deformation shapes in 100ºC: a) fundamental path, b) imperfections at points D, D', E, c) imperfections at points C, F

From the practical point of view the secondary path connected with the bifurcation point at 80ºC (Figure 8) is of great importance. Additional studies proves, that this point is symmetric unstable, what is shown in Figure 11. This illustration demonstrates the behavior of one of the post-bifurcation degrees of freedom - the in-plane longitudinal translation (u_G) of the point G (Figure 7) - obtained for the perfect case and for imperfections situated at the points D and D'.

According to the present failure control the material is safe in the range of 0-100ºC if the fundamental or secondary path connected with the bifurcation point at 80ºC is considered. In the case of the post-critical path corresponding to the junction point at 82ºC the matrix cracking occurs at about 100ºC. The authors of [5], where only the primary path is analyzed, report that the material fails at 94ºC. It must be however stressed, that the failure results are strongly dependent on the location of control points. In the present study the stress state is monitored at four Gauss points in each element. Moreover, the physical single layer of the shell is divided into three sub-layers, whereas the two outer ones have the thickness equal to 0.01*H*. It is not clear, how the control points are distributed in the thickness direction in [5]. One can only suppose that the stress state is monitored there in 9 Gauss points, because of the 9-node element with selective reduced integration (SRI) usage. The supplementary analysis performed by the Authors with the application of 8SRI elements leads to the solution of the failure temperature at 96ºC. However, according to [52] the best convergence of stress results in 8- and 9-node elements is achieved at the points matching the uniform reduced integration scheme.

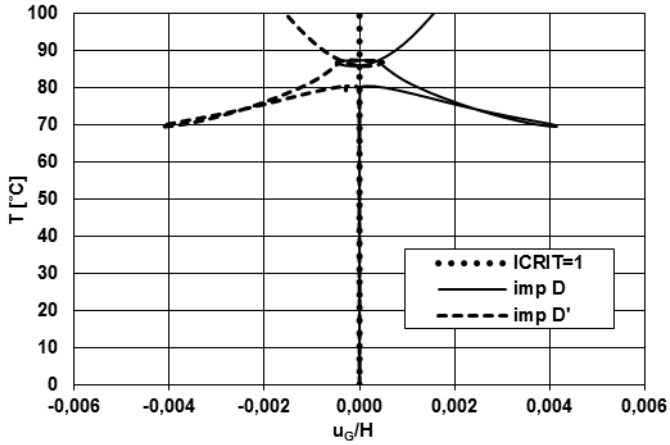

Fig. 11. Cylindrical shell. In-plane translation of point G; symmetrical unstable bifurcation point

4.4. *Cross-ply cylindrical thin shell under uniform thermal loading*

The example was proposed in [9, 11] and also investigated in [38]. A cylindrical panel with geometrical data $A=B=R\phi$, $\phi=15^{o}$, A/H=800 (Figure 5) under uniform thermal loading is analyzed. Three translations and rotations about the normal lines to the edges are fixed along all four edges. The shell is composed of four layers $[0^{o}/90^{o}]_{s}$ made of the same material as in the example 4.3.

Due to the significant *A/H* ratio one has to take care of the appropriate mesh density used in the computations. Considerable quality changes of the solutions were observed during the present convergence study. At least 20x20 8URI elements must be used to achieve the stabilization of the results. Nonetheless, as shown in Figure 12, the usage of such a mesh leads to completely different solution than reported by Oh and Lee [9, 11]. To verify the present solution obtained with the use of 8URI elements, an additional analysis was performed with the application of 16-node fully integrated finite elements (16FI). The agreement of two present results (Figure 12) indicates that the reference solution of [9, 11] and also of [38] can be incorrect.

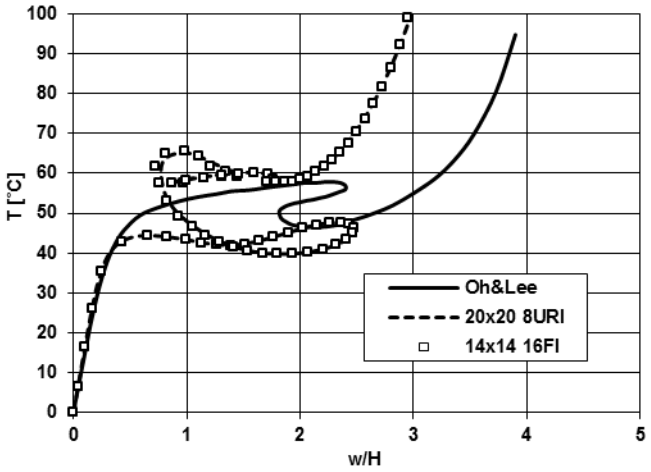

Fig. 12. Central deflection of the cross-ply cylindrical thin shell

Since the shell is very thin, one can suppose, that the results can be very much influenced by the shear locking. Thus the solution can strongly depend on the kind of element and mesh density applied in the computations.

In [9] and [38] 5x5 elements were used to discretize the quarter of the shell. In [9] the Hellinger-Reissner 9-node element was applied, whereas in [38] the 8-node Serendipity element with smoothed interpolation functions was adopted. The symmetry conditions were not applied in [11] and the 10x10 mesh of probably the same element as in [9] was employed. In the Authors' opinion, the solution error present in above mentioned works follows from too poor mesh density and shear locking.

To support this opinion, supplementary computations were performed by the Authors with the use of own 9-node fully integrated elements (9FI). Figure 13 demonstrates, that by applying the same mesh density as reported in [9, 11, 38] (10x10 9FI) almost the same path is obtained as the reference solution. However, as the mesh is condensed to 20x20 9FI elements, then the solution moves closer to that achieved with the mesh 20x20 of 8URI elements.

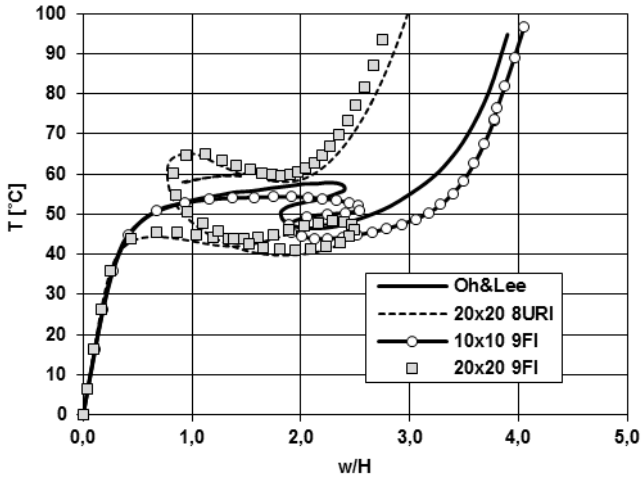

Fig. 13. The influence of discretization on the results

The obtained in the present study branch-type path with the several load limit and turning points occurring (Fig. 12-13) proves the dynamic and complex deformation of the shell which is caused by the significant slenderness of the structure. Since that the proper mesh of elements needs to be employed in the analysis to project the evolution of complicated deformation waves. Figures 14 and 15 show clearly, that the mesh density used in [9, 11, 38] is too poor for a proper representation of a thin shell deformation.

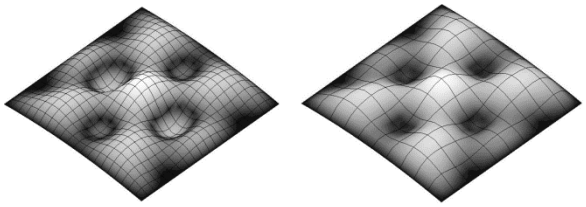

Fig. 14. Deformation shapes corresponding to w/H=1: a) 20x20 8URI elements, b) 10x10 9FI elements

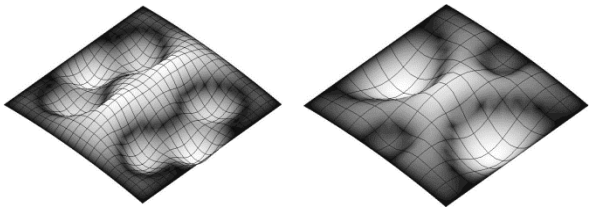

Fig. 15. Deformation shapes corresponding to 100ºC: a) 20x20 8URI elements, b) 10x10 9FI elements

The Tsai-Wu criterion in this example is not exceeded in the investigated range of temperatures.

4.5. *Spherical orthotropic shell under uniform temperature rise*

A nonlinear behavior of a spherical orthotropic panel subjected to a uniform temperature rise is analyzed in this example after [8]. The geometry of the shell (Figure 16) is characterized by the following data $A=B$, $A/H=200$, $R/A=6$. All edges are immovable to translate in three directions and to rotate about the normal lines to the edges. The material parameters are: $E_a=130\text{GPa}$, $E_b=7.0\text{GPa}$, $G_{ab}=G_{ac}=4.75\text{GPa}$, $G_{bc}=2.375\text{GPa}$, $\nu_{ab}=0.3$, $\alpha_{aa}^{th}=-0.3\cdot10^{-6}1/\text{K}$, $\alpha_{bb}^{th}=28.1\cdot10^{-6}\ 1/\text{K}$.

In the present computations 12x12 8URI elements were utilized. Figure 17 illustrates the equilibrium path for the normalized central deflection of the shell. It has to be noticed, that the normalization of deflections applied in Figure 17 (0.01wA/H) was changed when compared with (w/H) originally used in [8]. The Authors tested that such a modification provides a very good agreement of the present results with the reference solution for different values of *R/A*, what allows to make a conclusion of a possible printing error in [8].

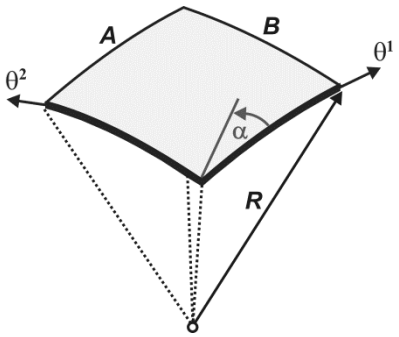

Fig. 16. Geometry of spherical shell

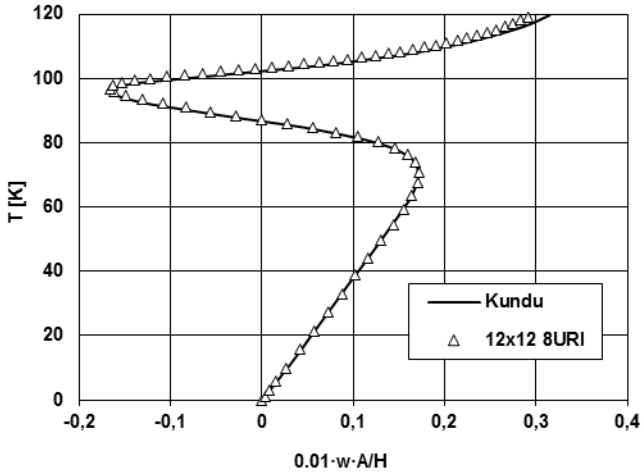

Fig. 17. Central deflection of spherical orthotropic shell

In supplementary studies the load distribution was modified, i.e. the influence of thermal gradients $T_b=0.5T_t$ and $T_t=0.5T_b$ on the structure's behavior was investigated. The results are presented in Figure 18. It is observed that both uniform heating ($T_b=T_t$) and gradient $T_b=0.5T_t$ do not cause the instability effects up to the 120K. Contrary the distribution $T_t=0.5T_b$ leads to snap-through in 112K.

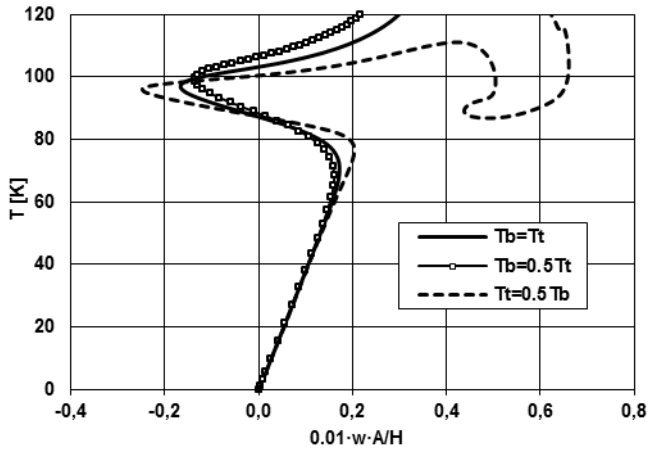

Fig. 18. The influence of load distribution on the structure stability

5.Conclusions

A numerical model of thermally loaded multilayered elastic plates and shells is presented in the paper. The main goal of the work is the stability study performed on the basis of the incremental nonlinear analysis, in which large displacements but small strains are assumed.

To extend the information about the bearing capacity of the structure, in each step the stress state is controlled in accordance with the Tsai-Wu failure criterion.

The multilayered panel is analyzed as an equivalent single layer (ESL) within framework of the first-order shear deformation theory (FOSD). The global constitutive relations were established with enhanced Lamination Theory adequate for the FOSD theory. In order to trace arbitrary equilibrium paths the Riks-Wempner-Ramm algorithm is adopted with the use of two different unloading conditions for a better examination of post-bifurcation branches. All computations are performed with the Authors' own finite element method program.

Several numerical examples are presented as the illustration of possibilities of the proposed model. It is shown, that thermally influenced thin shells can be very sensitive to the buckling, thus during the analysis a special attention should be paid to such aspects, like an appropriate path tracing method, suitable mesh density, using of symmetry conditions. It is also exposed, that the bearing capacity of thin shells is dominated by stability problems.

Nonetheless, the Authors are aware of the fact, that the presented approach at this stage enables to perform only initial studies. From the practical point of view, one should also take into account such effects, like thermal degradation of material properties, delamination and progressive failure. Then the numerical results could be compared with experimental data.

ACKNOWLEDGEMENTS

This work was partly financed by the Polish Ministry of Science and Higher Education under Grant No. N N506 254237. This financial support is gratefully acknowledged.

REFERENCES

[1] L.W. Ko, Predictions of thermal buckling strengths of hypersonic aircraft sandwich panels using minimum potential energy and finite element methods, NASA Technical Memorandum (1995) 4643.

[2] Y.I. Dimitrienko, Thermomechanical behaviour of composite materials and structures under high temperatures: 1. Materials, Compos. Part A 28A (1997) 453-461.

[3] A.K. Noor, W.S. Burton, Computational models for high-temperature multilayered composite plates and shells, Appl. Mech. Rev. 45 (1992) 419-445.
[4] A. Sabik, I. Kreja, Numerical analysis of laminated shells under in-plane axial compression, Proc. Appl. Math. Mech. 9 (2009) 251-252.
[5] N.N. Huang, T.R. Tauchert, Large deflections of laminated cylindrical and doubly-curved panels under thermal loading, Comput. Struct. 41 (1991) 303-312.
[6] A. Sabik, I. Kreja, Imperfection sensitivity of multilayered composite shells, in: W. Pietraszkiewicz, I. Kreja, (Eds.), Shell Structures: Theory and Applications Vol. 2, CRC Press/Balkema, London, 2010, pp. 137-140.
[7] A. Barut, E. Madenci, A. Tessler, Nonlinear thermoelastic analysis of composite panels under non-uniform temperature distribution, Int. J. Solids Struct. 37 (2000) 3681-3713.
[8] C.K. Kundu, J.H. Han, Nonlinear buckling analysis of hygrothermoelastic composite shell panels using finite element method, Compos. Part B 40 (2009) 313-328.
[9] J.J Lee, I.K. Oh, I. Lee, C.H. Yeom, Thermal post-buckling behavior of patched laminated panels under uniform and non-uniform temperature distributions, Compos. Struct. 55 (2002) 137-145.
[10] E. Madenci, A. Barut, Thermal postbuckling analysis of cylindrically curved composite laminates with a hole, Int. J. Numer. Meth. Eng. 37 (1994) 2073-2091.
[11] I.K. Oh, I. Lee, Thermal snapping and vibration characteristics of cylindrical composite panels using layerwise theory, Compos. Struct. 51 (2001) 49-61.
[12] A. Sabik, Stability analysis of thermally loaded multilayered shells (in Polish), Monographs of Gdansk University of Technology vol. 126, Gdańsk, Poland, 2012.
[13] M.K. Singha, L.S. Ramachandra, J.N. Bandyopadhyay, Nonlinear response of laminated cylindrical shell panels subjected to thermomechanical loads, J. Eng. Mech. 10 (2006) 1088-1095.
[14] G. Srikanth, A. Kumar, Postbuckling response and failure of symmetric laminates under uniform temperature rise, Compos. Struct. 1 (2003) 109-118.
[15] A. Avci, Ö.S. Sahin, N. Ataberk, Thermal buckling behavior of cross-ply hybrid composite laminates with inclined crack, Compos. Sci. Technol. 66 (2006) 2965-2970.
[16] J. Lee, Thermally induced buckling of laminated composites by a layerwise theory, Comput. Struct. 65 (1997) 917-922.
[17] H.R.H. Kabir, H. Askar, R.A. Chaudhuri, Thermal buckling response of shear flexible laminated anisotropic plates using a three-node isoparametric element, Compos. Struct. 59 (2003) 173-187.
[18] T. Kant, C.S. Babu, Thermal buckling analysis of skew fibre-reinforced composite and sandwich plates using shear deformable finite element models, Compos. Struct. 49 (2000) 77-85.
[19] A. Lal, B.N Singh, S. Kale, Stochastic post buckling analysis of laminated composite cylindrical shell panel subjected to hygrothermomechanical loading, Compos. Struct. 93 (2011) 1187-1200.
[20] J.F. Rakow, A.M. Waas, Thermal buckling of metal foam sandwich panels for convective thermal protection systems, J. Spacecraft Rockets 42 (2005) 832-844.
[21] R.M. Jones, Thermal buckling of uniformly heated unidirectional and symmetric cross-ply laminated fiber-reinforced composite uniaxial in-plane restrained simply supported rectangular plates, Compos. Part A 36 (2005) 1355-1367.
[22] S. Xiaoping, S. Liangxin, Thermomechanical buckling of laminated composite plates with higher-order transverse shear deformation, Comput. Struct. 53 (1994) 1-7.
[23] M.K. Singha, L.S. Ramachandra, J.N. Bandyopadhyay, Thermal postbuckling analysis of laminated composite plates, Compos. Struct. 54 (2001) 453-458.
[24] V.S. Thankam, G. Singh, R. Venkateswara, A.K. Rath, Thermal post-buckling behaviour of laminated plates using a shear-flexible element based on couple-displacement field, Compos. Struct. 59 (2003) 351-359.
[25] R. Pandey, K.K Shukla, A. Jain, Thermoelastic stability analysis of laminated composite plates: An analytical approach, Commun. Nonlinear Sci. Numer. Simul. 14 (2009) 1679-1699.
[26] K.K Shukla, Y. Nath, Analytical solution for buckling and post-buckling of angle-ply laminated plates under thermomechanical loading, Int. J. Nonlinear Mech. 36 (2001) 1097-1108.
[27] J. Argyris, R. Tenek, Postbuckling of composite laminates under compressive load and temperature, Comput. Meth. Appl. Mech. Eng. 128 (1995) 49-80.
[28] T. Hause, T. Librescu, Non-linear response of geometrically imperfect sandwich curved panels under thermomechanical loading, Int. J. Nonlinear Mech. 33 (1998) 1039-1059.
[29] L. Librescu, T. Hause, Recent developments in the modeling and behavior of advanced sandwich constructions: a survey, Compos. Struct. 48 (2000) 1-17.
[30] L. Librescu, W. Lin, Non-linear response of laminated plates and shells to thermomechanical loading: Implications of violation of interlaminar shear traction continuity requirement, Int. J. Solids Struct. 36 (1999) 4111-4147.
[31] A.K. Noor, J.H. Starnes, J.M. Peters, Nonlinear and postbuckling responses of curved composite panels with cutouts, Compos. Struct. 34 (1996) 213-240.
[32] M. Shariyat, Non-linear dynamic thermo-mechanical buckling analysis of the imperfect laminated and sandwich cylindrical shells based on a global-local theory inherently suitable for non-linear analyses, Int. J. Nonlinear Mech. 46 (2011) 253-271.
[33] H.S. Shen, Thermomechanical post-buckling analysis of imperfect laminated plates using a higher-order shear-deformation theory, Comput. Struct. 66 (1998) 395-409.

[34] H.S. Shen, Q.S. Li, Thermomechanical postbuckling of shear deformable laminated cylindrical shells with local geometric imperfections, Int. J. Solids Struct. 39 (2002) 4525-4542.
[35] B. Ruixiang, C. Haoran, Nonlinear buckling behavior of damaged composite sandwich plates considering the effect of temperature-dependent thermal and mechanical properties, Acta Mech. Solida Sin. 14 (2001) 155-160.
[36] M. Shariyat, Thermal buckling analysis of rectangular composite plates with temperature-dependent properties based on a layerwise theory, Thin Wall. Struct. 45 (2007) 439-452.
[37] H.S. Shen, Thermal postbuckling behavior of imperfect shear deformable laminated plates with temperature-dependent properties, Comput. Meth. Appl. Mech. Eng. 190 (2001) 5377-5390.
[38] R.M. Joshi, B.P. Patel, Nonlinear thermoelastic response of laminated conical panels, Struct. Eng. Mech. 34 (2010) 97-107.
[39] P.K. Gotsis, J.D. Guptill, Fiber composite thin shells subjected to thermal buckling loads, Comput. Struct. 53 (1994) 1263-1274.
[40] I.K. Oh, I. Lee, Non-linear transient response of fluttering stiffened composite plates subject to thermal load, J. Sound Vib. 245 (2001) 715-736.
[41] K.J. Bathe, Finite-Elemente-Methoden, Matrizen und lineare Algebra, die Methode der finiten Elemente, Lösung von Gleichgewichtsbedingungen und Bewegungsgleichungen, Springer-Verlag, Berlin Heidelberg, 1986.
[42] A. Wetzel, L. Kärger, R. Rolfes, K. Rohwer, Evaluation of two finite element formulations for a rapid 3D stress analysis of sandwich structures, Comput. Struct. 83 (2005) 1537-1545.
[43] I. Kreja, A literature review on computational models for laminated composite and sandwich panels, Cent. Eur. J. Eng. 1 (2011) 59-80.
[44] J.N. Reddy, Mechanics of laminated composite plates and shells. Theory and analysis, 2nd ed., CRC Press, Philadelphia, 2004.
[45] R.M. Jones, Mechanics of composite materials, 2nd ed., Taylor&Francis, London, 1999.
[46] A. Sabik, I. Kreja, The analysis of laminated plates with the use of equivalent single layer models (in Polish), Acta Mechanica et Automatica 2 (2008) 63-68.
[47] S. Vlachoutsis, Shear correction factors for plates and shells, Int. J. Numer. Meth. Eng. 33 (1992) 1537-1552.
[48] J. Whitney, Shear correction factors for orthotropic laminates under static load, J. Appl. Mech.-T ASME 40 (1973) 302-303.
[49] E. Ramm, The Riks/Wempner approach - an extension of the displacement control method in nonlinear analyses, Recent Advances in Non-linear Computational Mechanics, Pineridge Press Ltd, Swansea, 1982, pp. 62-86.
[50] E.Jr. Parente, A.S. de Holanda, S.M.B. Afonso da Silva, Tracing nonlinear equilibrium paths of structures subjected to thermal loading, Comput. Mech. 38 (2006) 505-520.
[51] I. Kreja, R. Schmidt, J.N. Reddy, Finite elements based on a first-order shear deformation moderate rotation shell theory with applications to the analysis of composite structures, Int. J. Nonlinear Mech. 36 (1996) 1123-1142.
[52] X. Zhang, Why do Barlow points not coincide with the reduced Gauss quadrature points for higher-order finite elements?, Commun. Numer. Meth. Eng. 24 (2008) 1251-1256.
[53] Y. Başar, W. Krätzig, Theory of shell structures, 2. Auflage, VDI Verlag GmbH, Düsseldorf, 2001.
[54] J. Chróścielewski, J. Makowski, W. Pietraszkiewicz, Static and dynamics of multi-shell structures. Non-linear theory and FEM (in Polish), IFTR PASci, Warsaw, 2004.
[55] J. Chróścielewski, W. Witkowski, Four-node semi-EAS element in 6-field nonlinear theory of shells, Int. J. Numer. Meth. Eng. 68 (2006) 1137-1179.
[56] J. Chróścielewski, I. Kreja, A. Sabik, W. Witkowski, Modeling of composite shells in 6–parameter nonlinear theory with drilling degree of freedom, Mech. Adv. Mat. Struct. 18 (2011) 403-419.
[57] I. Kreja, R. Schmidt, Large rotations in first-order shear deformation FE analysis of laminated shells, Int. J. Nonlinear Mech. 41 (2006) 101-123.
[58] B. Bouhafs, K. Woźnica, P. Kłosowski, The large rotations theory of elasto-viscoplastic shells subjected to dynamic and thermal loads, Eng. Computation 20 (2003) 366-389.

APPENDIX A

The shell kinematics

In the following formulas the Greek indices are equal to 1 or 2, whereas the Latin ones are 1, 2 or 3.

The FOSD formulation states, that a straight and normal line remains straight but not necessarily normal during the deformation, see Figure A.1. The position vectors of an

arbitrary point P^* of the shell in the initial (t=0) and actual (t=m) configuration can be expressed in the following form:

$$ {}^{0}\mathbf{R}(\theta^1,\theta^2,\theta^3) = {}^{0}\mathbf{r}(\theta^1,\theta^2) + \theta^3\,{}^{0}\mathbf{n}(\theta^1,\theta^2)\,, \tag{A.1} $$

$$ {}^{m}\mathbf{R}(\theta^1,\theta^2,\theta^3) = {}^{m}\mathbf{r}(\theta^1,\theta^2) + \theta^3\,{}^{m}\mathbf{d}(\theta^1,\theta^2)\,, \tag{A.2} $$

where ${}^{0}\mathbf{n}$ and ${}^{m}\mathbf{d}$ are the normal vector in the initial configuration and so called director in the configuration m, which is not necessarily perpendicular to the middle surface of the shell.

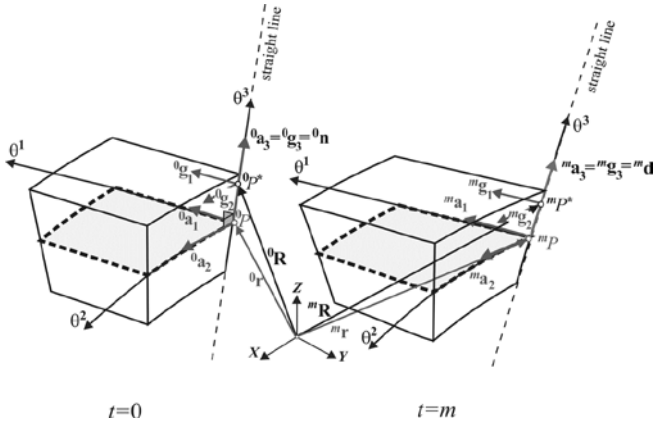

Fig. A.1. Geometry of the shell

The displacement vector of an arbitrary point P^* comes out from:

$$ {}^{m}\mathbf{V} = {}^{m}\mathbf{R} - {}^{0}\mathbf{R} \quad \Leftrightarrow \quad {}^{m}\mathbf{V} = ({}^{m}\mathbf{r} - {}^{0}\mathbf{r}) + \theta^3({}^{m}\mathbf{d} - {}^{0}\mathbf{n}) = \overset{(0)}{{}^{m}\mathbf{V}} + \theta^3\,\overset{(1)}{{}^{m}\mathbf{V}}\,. \tag{A.3} $$

In the Total Lagrangian formulation the displacement vector can be decomposed as follows

$$ {}^{m}\mathbf{V} = {}^{m}\upsilon^{\alpha}\,{}^{0}\mathbf{a}_{\alpha} + {}^{m}\upsilon^{3}\,{}^{0}\mathbf{n} = {}^{m}\upsilon_{\alpha}\,{}^{0}\mathbf{a}^{\alpha} + {}^{m}\upsilon_{3}\,{}^{0}\mathbf{n}\,. \tag{A.4} $$

In a scalar description, the displacement components can be expressed as

$$ {}^{m}\upsilon_i(\theta^1,\theta^2,\theta^3) = \overset{(0)}{{}^{m}\upsilon_i}(\theta^1,\theta^2) + \theta^3\,\overset{(1)}{{}^{m}\upsilon_i}(\theta^1,\theta^2)\,. \tag{A.5} $$

One should notice that 6 scalar parameters are present in (A.5). Furthermore, it must be stressed that the sixth parameter in this case is associated with the transverse normal stretching. The last remark is very important, because in some other formulations the sixth parameter plays completely different role, namely serves as so called drilling rotation [54-56].

The components of Green-Lagrange strain tensor can be expressed in terms of metric tensor components [53], namely

$$2\,{}^{m}_{0}E_{ij} = {}^{m}g_{ij} - {}^{0}g_{ij}\,. \tag{A.6}$$

By separating the membrane, transverse shear and transverse normal parts in the strain tensor one gets the following expressions

$$\begin{aligned}
&{}^{m}_{0}E_{\alpha\beta}(\theta^1,\theta^2,\theta^3) = {}^{m}_{0}\overset{(0)}{E}_{\alpha\beta}(\theta^1,\theta^2) + \theta^3\,{}^{m}_{0}\overset{(1)}{E}_{\alpha\beta}(\theta^1,\theta^2) + \left(\theta^3\right)^2\,{}^{m}_{0}\overset{(2)}{E}_{\alpha\beta}(\theta^1,\theta^2),\\
&{}^{m}_{0}E_{\alpha 3}(\theta^1,\theta^2,\theta^3) = {}^{m}_{0}\overset{(0)}{E}_{\alpha 3}(\theta^1,\theta^2) + \theta^3\,{}^{m}_{0}\overset{(1)}{E}_{\alpha 3}(\theta^1,\theta^2),\\
&{}^{m}_{0}E_{33}(\theta^1,\theta^2,\theta^3) = {}^{m}_{0}\overset{(0)}{E}_{33}(\theta^1,\theta^2).
\end{aligned} \tag{A.7}$$

Taking into account, that the covariant base vectors at an arbitrary point P^* obtained from (A.1) and (A.2) are following

$$\begin{aligned}
&{}^{m}\mathbf{g}_{\alpha} = {}^{m}\mathbf{a}_{\alpha} + \theta^3\,{}^{m}\mathbf{d}_{,\alpha}\,,\\
&{}^{m}\mathbf{g}_{3} = {}^{m}\mathbf{d},\\
&{}^{0}\mathbf{g}_{\alpha} = {}^{0}\mathbf{a}_{\alpha} + \theta^3\,{}^{0}\mathbf{n}_{,\alpha}\,,\\
&{}^{0}\mathbf{g}_{3} = {}^{0}\mathbf{n},
\end{aligned} \tag{A.8}$$

the components of the strains in (A.7) result from:

$$\begin{aligned}
&2\,{}^{m}_{0}\overset{(0)}{E}_{\alpha\beta}(\theta^1,\theta^2) = {}^{m}\mathbf{a}_{\alpha}\cdot{}^{m}\mathbf{a}_{\beta} - {}^{0}\mathbf{a}_{\alpha}\cdot{}^{0}\mathbf{a}_{\beta},\\
&2\,{}^{m}_{0}\overset{(1)}{E}_{\alpha\beta}(\theta^1,\theta^2) = {}^{m}\mathbf{d}_{,\alpha}\cdot{}^{m}\mathbf{a}_{\beta} + {}^{m}\mathbf{a}_{\alpha}\cdot{}^{m}\mathbf{d}_{,\beta} - {}^{0}\mathbf{n}_{,\alpha}\cdot{}^{0}\mathbf{a}_{\beta} - {}^{0}\mathbf{a}_{\alpha}\cdot{}^{0}\mathbf{n}_{,\beta}\,,\\
&2\,{}^{m}_{0}\overset{(2)}{E}_{\alpha\beta}(\theta^1,\theta^2) = {}^{m}\mathbf{d}_{,\alpha}\cdot{}^{m}\mathbf{d}_{,\beta} - {}^{0}\mathbf{n}_{,\alpha}\cdot{}^{0}\mathbf{n}_{,\beta}\,,\\
&\\
&2\,{}^{m}_{0}\overset{(0)}{E}_{\alpha 3}(\theta^1,\theta^2) = {}^{m}\mathbf{a}_{\alpha}\cdot{}^{m}\mathbf{d},\\
&2\,{}^{m}_{0}\overset{(1)}{E}_{\alpha 3}(\theta^1,\theta^2) = {}^{m}\mathbf{d}_{,\alpha}\cdot{}^{m}\mathbf{d},\\
&\\
&2\,{}^{m}_{0}\overset{(0)}{E}_{33}(\theta^1,\theta^2) = {}^{m}\mathbf{d}\cdot{}^{m}\mathbf{d} - 1.
\end{aligned} \tag{A.9}$$

In (A.9) the transverse stretching is present. However, in the FOSD formulation it is usually assumed that the fibers are inextensible in the transverse normal direction, what can be also interpreted (c.f. [57]) as

$${}^{m}_{0}E_{33} = 0 \quad\Rightarrow\quad {}^{m}\mathbf{d}\cdot{}^{m}\mathbf{d} = 1 \quad\Rightarrow\quad {}^{m}\mathbf{d}_{,\alpha}\cdot{}^{m}\mathbf{d} = 0\,, \tag{A.10}$$

what implies that the transverse shear strain is constant in the thickness direction.

Obviously, the displacement state (A.5) can be also simplified as the sixth displacement parameter is omitted

$$
\begin{aligned}
&{}^{m}\upsilon_{\alpha}(\theta^1,\theta^2,\theta^3) = {}^{m}\overset{(0)}{\upsilon}_{\alpha}(\theta^1,\theta^2) + \theta^3\,{}^{m}\overset{(1)}{\upsilon}_{\alpha}(\theta^1,\theta^2),\\
&{}^{m}\upsilon_{3}(\theta^1,\theta^2,\theta^3) = {}^{m}\overset{(0)}{\upsilon}_{3}(\theta^1,\theta^2) = const.
\end{aligned}
\tag{A.11}
$$

Finally the displacement-strain relations in the 5-parameter theory can be expressed in the following form

$$
\begin{aligned}
&2\,{}^{m}_{0}\overset{(0)}{E}_{\alpha\beta} = {}^{m}\overset{(0)}{\varphi}_{\beta\alpha} + {}^{m}\overset{(0)}{\varphi}_{\alpha\beta} + {}^{m}\overset{(0)}{\varphi}_{\delta\alpha}\,{}^{m}\overset{(0)}{\varphi}{}^{\delta}_{\beta} + {}^{m}\overset{(0)}{\varphi}_{\alpha 3}\,{}^{m}\overset{(0)}{\varphi}_{\beta 3},\\
&2\,{}^{m}_{0}\overset{(1)}{E}_{\alpha\beta} = {}^{m}\overset{(1)}{\upsilon}_{\beta}\big|_{\alpha} + {}^{m}\overset{(1)}{\upsilon}_{\alpha}\big|_{\beta} - {}^{0}b^{\lambda}_{\alpha}\,{}^{m}\overset{(0)}{\varphi}_{\lambda\beta} - {}^{0}b^{\lambda}_{\beta}\,{}^{m}\overset{(0)}{\varphi}_{\lambda\alpha} + {}^{m}\overset{(1)}{\upsilon}_{\delta}\big|_{\alpha}\,{}^{m}\overset{(0)}{\varphi}{}^{\delta}_{\beta} + {}^{m}\overset{(1)}{\upsilon}_{\delta}\big|_{\beta}\,{}^{m}\overset{(0)}{\varphi}{}^{\delta}_{\alpha} +\\
&\qquad + {}^{m}\overset{(0)}{\varphi}_{\beta 3}\,{}^{m}\overset{(1)}{\upsilon}_{\lambda}\,{}^{0}b^{\lambda}_{\alpha} + {}^{m}\overset{(0)}{\varphi}_{\alpha 3}\,{}^{m}\overset{(1)}{\upsilon}_{\lambda}\,{}^{0}b^{\lambda}_{\beta},\\
&2\,{}^{m}_{0}\overset{(2)}{E}_{\alpha\beta} = -{}^{0}b^{\lambda}_{\alpha}\,{}^{m}\overset{(1)}{\upsilon}_{\lambda}\big|_{\beta} - {}^{0}b^{\delta}_{\beta}\,{}^{m}\overset{(1)}{\upsilon}_{\delta}\big|_{\alpha} + {}^{m}\overset{(1)}{\upsilon}{}^{\lambda}\big|_{\alpha}\,{}^{m}\overset{(1)}{\upsilon}_{\lambda}\big|_{\beta} + \left({}^{m}\overset{(1)}{\upsilon}_{\delta}\,{}^{0}b^{\delta}_{\alpha}\right)\left({}^{m}\overset{(1)}{\upsilon}_{\lambda}\,{}^{0}b^{\lambda}_{\beta}\right),\\
&2\,{}^{m}_{0}\overset{(0)}{E}_{\alpha 3} = {}^{m}\overset{(1)}{\upsilon}_{\alpha} + {}^{m}\overset{(0)}{\varphi}_{\alpha 3} + {}^{m}\overset{(0)}{\varphi}{}^{\lambda}_{\alpha}\,{}^{m}\overset{(1)}{\upsilon}_{\lambda},
\end{aligned}
\tag{A.12}
$$

where

$$
\begin{aligned}
&{}^{m}\overset{(0)}{\varphi}_{\alpha\beta} = {}^{m}\overset{(0)}{\upsilon}_{\alpha}\big|_{\beta} - {}^{m}\overset{(0)}{\upsilon}_{3}\,{}^{0}b_{\alpha\beta},\\
&{}^{m}\overset{(1)}{\varphi}_{\alpha\beta} = {}^{m}\overset{(1)}{\upsilon}_{\alpha}\big|_{\beta} - {}^{m}\overset{(1)}{\upsilon}_{3}\,{}^{0}b_{\alpha\beta} = {}^{m}\overset{(1)}{\upsilon}_{\alpha}\big|_{\beta},
\end{aligned}
$$

$$
\begin{aligned}
&{}^{m}\overset{(0)}{\varphi}_{\alpha 3} = {}^{m}\overset{(0)}{\upsilon}_{\lambda}\,{}^{0}b^{\lambda}_{\alpha} + {}^{m}\overset{(0)}{\upsilon}_{3,\alpha},\\
&{}^{m}\overset{(1)}{\varphi}_{\alpha 3} = {}^{m}\overset{(1)}{\upsilon}_{\lambda}\,{}^{0}b^{\lambda}_{\alpha} + {}^{m}\overset{(1)}{\upsilon}_{3,\alpha} = {}^{m}\overset{(1)}{\upsilon}_{\lambda}\,{}^{0}b^{\lambda}_{\alpha},
\end{aligned}
\tag{A.13}
$$

$$
\begin{aligned}
&{}^{m}\overset{(0)}{\varphi}{}^{\delta}_{\beta} = {}^{m}\overset{(0)}{\varphi}_{\beta\lambda}\,{}^{0}a^{\delta\lambda} = {}^{m}\overset{(0)}{\upsilon}{}^{\delta}\big|_{\beta} - {}^{m}\overset{(0)}{\upsilon}_{3}\,{}^{0}b^{\delta}_{\beta},\\
&{}^{m}\overset{(1)}{\varphi}{}^{\delta}_{\beta} = {}^{m}\overset{(1)}{\varphi}_{\beta\lambda}\,{}^{0}a^{\delta\lambda} = {}^{m}\overset{(1)}{\upsilon}{}^{\delta}\big|_{\beta} - {}^{m}\overset{(1)}{\upsilon}_{3}\,{}^{0}b^{\delta}_{\beta} = {}^{m}\overset{(1)}{\upsilon}{}^{\delta}\big|_{\beta}.
\end{aligned}
$$

The vertical line in (A.12) and (A.13) stands for the covariant differentiation of displacement vector components [53].

It must be noticed that above displacement-strain relations are inadequate within a proper description of finite rotations [57]; however, it is assumed that the magnitude of rotations in the thermo-elastic problems considered in this work is considerably limited, as compared with

the case of shells under an arbitrary mechanical loading [56]. Similar assumption was made by the authors of [58].

APPENDIX B

Incremental decomposition of virtual work

According to the virtual work principle we can postulate equilibrium of the internal and external virtual work in the unknown configuration:

$$ {}^{2}\delta W_i = {}^{2}\delta W_e \tag{B.1}$$

The external work corresponds to the activity of external mechanical forces, which are not considered in this work, so that the detail discussion about this term will be omitted.

The internal work in the unknown configuration has the following representation

$$ {}^{2}\delta W_i = \int_{{}^{2}V} {}^{2}_{2}\sigma^{ij}_{ef}\,\delta\, {}^{2}_{2}e_{ij}\, {}^{2}dV = \int_{{}^{2}V} \left({}^{2}_{2}\sigma^{ij}_{mech} - {}^{2}_{2}\sigma^{ij}_{th} \right) \delta\, {}^{2}_{2}e_{ij}\, {}^{2}dV \,, \tag{B.2}$$

where the Cauchy stress and Euler-Almansi strain measures are employed, which are not suitable for the Total Lagrangian description. After the appropriate [12] transformation one can rewrite the formula (B.2) in terms of the 2-nd Piola-Kirchhoff stress and Green-Lagrange strain tensors:

$$ {}^{2}\delta W_i = \int_{{}^{2}V} \left({}^{2}_{2}\sigma^{ij}_{mech} - {}^{2}_{2}\sigma^{ij}_{th} \right) \delta\, {}^{2}_{2}e_{ij}\, {}^{2}dV = \int_{{}^{0}V} \left({}^{2}_{0}S^{mn}_{mech} - {}^{2}_{0}S^{mn}_{th} \right) \delta\, {}^{2}_{0}E_{mn}\, {}^{0}dV \,. \tag{B.3}$$

By decomposing of the stress and strain tensors one can transform (B.3) into

$$ {}^{2}\delta W_i = \int_{{}^{0}V} \left(\left({}^{1}_{0}S^{mn}_{mech} + {}_{0}S^{mn}_{mech} \right) - {}^{2}_{0}S^{mn}_{th} \right) \delta\, {}_{0}E_{mn}\, {}^{0}dV \,, \tag{B.4}$$

where $\delta\, {}_{0}E_{mn}$ is the variation of the Green-Lagrange strain tensor.

In the ESL concept the integration in the thickens direction (H) in (B.4) is separated from the integration in plane (Ω):

$$ {}^{2}\delta W_i = \int_{{}^{0}\Omega} \int_{{}^{0}H} \left\{ \left({}^{1}_{0}S^{mn}_{mech} + {}_{0}S^{mn}_{mech} \right) - {}^{2}_{0}S^{mn}_{th} \right\} \delta\, {}_{0}E_{mn}\, {}^{0}\mu\, {}^{0}dH\, {}^{0}d\Omega \,, \tag{B.5}$$

where ${}^{0}\mu$ is the determinant of the shifter tensor [12, 53].

Finally, from the pre-integration of 3-D stress measures in (B.5), it follows, that

$$ {}^{2}\delta W_i = \int_{{}^{0}\Omega} \left\{ \sum_{n=0}^{2} \delta \, {}_{0}^{(n)}E_{\alpha\beta} \left(\left({}_{0}^{1}L_{mech}^{(n)\alpha\beta} + {}_{0}L_{mech}^{(n)\alpha\beta} \right) - {}_{0}^{2}L_{th}^{(n)\alpha\beta} \right) + 2\delta \, {}_{0}^{(0)}E_{\alpha 3} \left({}_{0}^{1}L_{mech}^{(0)\alpha 3} + {}_{0}L_{mech}^{(0)\alpha 3} \right) \right\} {}^{0}d\Omega \, . \tag{B.6} $$

In (B.6) ${}_{0}^{1}L_{mech}^{(n)\alpha\beta}$, ${}_{0}^{1}L_{mech}^{(0)\alpha 3}$ stand for the actual membrane-bending and transverse shear resultant forces:

$$ \left\{ {}_{0}^{1}\mathcal{N}_{mech} \right\} = \left\{ \begin{matrix} {}_{0}^{1}L_{mech}^{(0)11} \\ {}_{0}^{1}L_{mech}^{(0)22} \\ {}_{0}^{1}L_{mech}^{(0)12} \end{matrix} \right\}, \qquad \left\{ {}_{0}^{1}\mathcal{M}_{mech} \right\} = \left\{ \begin{matrix} {}_{0}^{1}L_{mech}^{(1)11} \\ {}_{0}^{1}L_{mech}^{(1)22} \\ {}_{0}^{1}L_{mech}^{(1)12} \end{matrix} \right\}, \qquad \left\{ {}_{0}^{1}\mathcal{B}_{mech} \right\} = \left\{ \begin{matrix} {}_{0}^{1}L_{mech}^{(2)11} \\ {}_{0}^{1}L_{mech}^{(2)22} \\ {}_{0}^{1}L_{mech}^{(2)12} \end{matrix} \right\}, $$

$$ \left\{ {}_{0}^{1}\mathcal{Q}_{mech} \right\} = \left\{ \begin{matrix} {}_{0}^{1}L_{mech}^{(0)23} \\ {}_{0}^{1}L_{mech}^{(0)13} \end{matrix} \right\}, \tag{B.7} $$

${}_{0}^{(n)}L_{mech}^{\alpha\beta}$, ${}_{0}^{(0)}L_{mech}^{\alpha 3}$ are their corresponding increments:

$$ \left\{ {}_{0}\mathcal{N}_{mech} \right\} = \left\{ \begin{matrix} {}_{0}^{(0)}L_{mech}^{11} \\ {}_{0}^{(0)}L_{mech}^{22} \\ {}_{0}^{(0)}L_{mech}^{12} \end{matrix} \right\}, \qquad \left\{ {}_{0}\mathcal{M}_{mech} \right\} = \left\{ \begin{matrix} {}_{0}^{(1)}L_{mech}^{11} \\ {}_{0}^{(1)}L_{mech}^{22} \\ {}_{0}^{(1)}L_{mech}^{12} \end{matrix} \right\}, \qquad \left\{ {}_{0}\mathcal{B}_{mech} \right\} = \left\{ \begin{matrix} {}_{0}^{(2)}L_{mech}^{11} \\ {}_{0}^{(2)}L_{mech}^{22} \\ {}_{0}^{(2)}L_{mech}^{12} \end{matrix} \right\}, $$

$$ \left\{ {}_{0}\mathcal{Q}_{mech} \right\} = \left\{ \begin{matrix} {}_{0}^{(0)}L_{mech}^{23} \\ {}_{0}^{(0)}L_{mech}^{13} \end{matrix} \right\}, \tag{B.8} $$

and ${}_{0}^{2}L_{th}^{(n)\alpha\beta}$ are the thermal resultant forces:

$$ \left\{ {}_{0}^{2}\mathcal{N}_{th} \right\} = \left\{ \begin{matrix} {}_{0}^{2}L_{th}^{(0)11} \\ {}_{0}^{2}L_{th}^{(0)22} \\ {}_{0}^{2}L_{th}^{(0)12} \end{matrix} \right\}, \qquad \left\{ {}_{0}^{2}\mathcal{M}_{th} \right\} = \left\{ \begin{matrix} {}_{0}^{2}L_{th}^{(1)11} \\ {}_{0}^{2}L_{th}^{(1)22} \\ {}_{0}^{2}L_{th}^{(1)12} \end{matrix} \right\}, \qquad \left\{ {}_{0}^{2}\mathcal{B}_{th} \right\} = \left\{ \begin{matrix} {}_{0}^{2}L_{th}^{(2)11} \\ {}_{0}^{2}L_{th}^{(2)22} \\ {}_{0}^{2}L_{th}^{(2)12} \end{matrix} \right\}. \tag{B.9} $$

The pre-integration of the 3-D stress measures leads to the constitutive relations at the cross-section level and for the mechanical part we have:

$$\left\{ {}_0\boldsymbol{S}_{mech} \right\} = \left[{}_0\boldsymbol{\mathcal{H}}_{mech} \right] \left\{ {}_0\boldsymbol{\mathcal{E}}_{mech} \right\}, \tag{B.10}$$

where

$$\left\{ {}_0\boldsymbol{S}_{mech} \right\} = \begin{Bmatrix} \left\{ {}_0\boldsymbol{\mathcal{N}}_{mech} \right\} \\ \left\{ {}_0\boldsymbol{\mathcal{M}}_{mech} \right\} \\ \left\{ {}_0\boldsymbol{\mathcal{B}}_{mech} \right\} \\ \left\{ {}_0\boldsymbol{\mathcal{Q}}_{mech} \right\} \end{Bmatrix}, \qquad \left\{ {}_0\boldsymbol{\mathcal{E}}_{mech} \right\} = \begin{Bmatrix} \left\{ {}_0\boldsymbol{\varepsilon}^{(0)} \right\} \\ \left\{ {}_0\boldsymbol{\varepsilon}^{(1)} \right\} \\ \left\{ {}_0\boldsymbol{\varepsilon}^{(2)} \right\} \\ \left\{ {}_0\boldsymbol{\gamma}^{(0)} \right\} \end{Bmatrix}. \tag{B.11}$$

The constitutive matrix $\left[{}_0\boldsymbol{\mathcal{H}}_{mech} \right]$ has the following structure

$$\left[{}_0\boldsymbol{\mathcal{H}}_{mech} \right] = \begin{bmatrix} {}^{(0,0)}[A]_{3\times3} & {}^{(0,1)}[B]_{3\times3} & {}^{(0,2)}[D]_{3\times3} & [0]_{3\times2} \\ {}^{(1,0)}[B]_{3\times3} & {}^{(1,1)}[D]_{3\times3} & {}^{(1,2)}[E]_{3\times3} & [0]_{3\times2} \\ {}^{(2,0)}[D]_{3\times3} & {}^{(2,1)}[E]_{3\times3} & {}^{(2,2)}[F]_{3\times3} & [0]_{3\times2} \\ [0]_{2\times3} & [0]_{2\times3} & [0]_{2\times3} & {}^{(0,0)}[S_A]_{2\times2} \end{bmatrix}, \tag{B.12}$$

where

$$[A]_{3\times3} = \begin{bmatrix} a_{11} & a_{12} & a_{13} \\ a_{21} & a_{22} & a_{23} \\ a_{31} & a_{32} & a_{33} \end{bmatrix}, \quad [S_A]_{2\times2} = \begin{bmatrix} k_{23}a_{44} & \sqrt{k_{23}k_{13}}\,a_{45} \\ \sqrt{k_{23}k_{13}}\,a_{54} & k_{13}a_{55} \end{bmatrix}, \quad a_{ij} = \int_{-\frac{H}{2}}^{\frac{H}{2}} c_{ij}\,{}^0\mu d\theta^3, \tag{B.13}$$

$$[B]_{3\times3} = \begin{bmatrix} b_{11} & b_{12} & b_{13} \\ b_{21} & b_{22} & b_{23} \\ b_{31} & b_{32} & b_{33} \end{bmatrix}, \quad b_{ij} = \int_{-\frac{H}{2}}^{\frac{H}{2}} c_{ij}\theta^3\,{}^0\mu d\theta^3, \tag{B.14}$$

$$[D]_{3\times3} = \begin{bmatrix} d_{11} & d_{12} & d_{13} \\ d_{21} & d_{22} & d_{23} \\ d_{31} & d_{32} & d_{33} \end{bmatrix}, \quad d_{ij} = \int_{-\frac{H}{2}}^{\frac{H}{2}} c_{ij}\left(\theta^3\right)^2\,{}^0\mu d\theta^3, \tag{B.15}$$

$$[E]_{3\times3} = \begin{bmatrix} e_{11} & e_{12} & e_{13} \\ e_{21} & e_{22} & e_{23} \\ e_{31} & e_{32} & e_{33} \end{bmatrix}, \quad e_{ij} = \int_{-\frac{H}{2}}^{\frac{H}{2}} c_{ij}\left(\theta^3\right)^3\,{}^0\mu d\theta^3, \tag{B.16}$$

$$[F]_{3\times3} = \begin{bmatrix} f_{11} & f_{12} & f_{13} \\ f_{21} & f_{22} & f_{23} \\ f_{31} & f_{32} & f_{33} \end{bmatrix}, \quad f_{ij} = \int_{-\frac{H}{2}}^{\frac{H}{2}} c_{ij}\left(\theta^3\right)^4\,{}^0\mu d\theta^3, \tag{B.17}$$

In (B.13)-(B.17) c_{ij} stands for the components of the constitutive matrix $[\mathrm{C}]$ (10). It is worth to notice, that the global transverse shear correction factors k_{13} and k_{23} are incorporated in block $[S_A]$ in (B.13) as declared in 2.2.

For the thermal part we get the analogical relations:

$$\left\{ {}^{2}_{0}\boldsymbol{S}_{th} \right\} = \left[{}_{0}\boldsymbol{\mathcal{H}}_{th} \right] \left\{ {}^{2}_{0}\boldsymbol{\mathcal{T}} \right\}, \tag{B.18}$$

where

$$\left\{ {}^{2}_{0}\boldsymbol{S}_{th} \right\} = \begin{Bmatrix} \left\{ {}^{2}_{0}\boldsymbol{\mathcal{N}}_{th} \right\} \\ \left\{ {}^{2}_{0}\boldsymbol{\mathcal{M}}_{th} \right\} \\ \left\{ {}^{2}_{0}\boldsymbol{\mathcal{B}}_{th} \right\} \\ \left\{ 0 \right\} \end{Bmatrix}, \qquad \left\{ {}^{2}_{0}\boldsymbol{\mathcal{T}} \right\} = \begin{Bmatrix} T^{(0)} \\ T^{(1)} \end{Bmatrix}, \tag{B.19}$$

with

$$\left[{}_{0}\boldsymbol{\mathcal{H}}_{th} \right] = \begin{bmatrix} \overset{(0,0)}{\{A_{th}\}}_{3\times1} & \overset{(0,1)}{\{B_{th}\}}_{3\times1} \\ \overset{(1,0)}{\{B_{th}\}}_{3\times1} & \overset{(1,1)}{\{D_{th}\}}_{3\times1} \\ \overset{(2,0)}{\{D_{th}\}}_{3\times1} & \overset{(2,1)}{\{E_{th}\}}_{3\times1} \\ \{0\}_{2\times1} & \{0\}_{2\times1} \end{bmatrix}. \tag{B.20}$$

The vectors included in $\left[{}_{0}\boldsymbol{\mathcal{H}}_{th} \right]$ have the following components

$$\left\{ A_{th} \right\}_{3x1} = \begin{Bmatrix} a^{1}_{th} \\ a^{2}_{th} \\ a^{3}_{th} \end{Bmatrix}, \qquad a^{i}_{th} = \int_{-\frac{h}{2}}^{\frac{h}{2}} c^{i}_{th}\, {}^{0}\mu d\theta^{3}, \tag{B.21}$$

$$\left\{ B_{th} \right\}_{3x1} = \begin{Bmatrix} b^{1}_{th} \\ b^{2}_{th} \\ b^{3}_{th} \end{Bmatrix}, \qquad b^{i}_{th} = \int_{-\frac{h}{2}}^{\frac{h}{2}} c^{i}_{th}\, \theta^{3}\, {}^{0}\mu d\theta^{3}, \tag{B.22}$$

$$\left\{ D_{th} \right\}_{3x1} = \begin{Bmatrix} d^{1}_{th} \\ d^{2}_{th} \\ d^{3}_{th} \end{Bmatrix}, \qquad d^{i}_{th} = \int_{-\frac{h}{2}}^{\frac{h}{2}} c^{i}_{th} \left(\theta^{3} \right)^{2}\, {}^{0}\mu d\theta^{3}, \tag{B.23}$$

where c^{i}_{th} are the components of the vector $\left\{ \mathrm{C}_{th} \right\}$ (10).

APPENDIX C

Incremental equilibrium equation

By employing the constitutive relations for the cross-section level, one can rewrite the equation (B.6) into

$$ {}^{2}\delta W_i = \int_{{}_0\Omega} \left[\sum_{n=0}^{2} \delta\, {}_0\overset{(n)}{E}_{\alpha\beta} \left\{ {}^{1}_{0}\overset{(n)}{L}{}^{\alpha\beta}_{mech} + \sum_{m=0}^{2} \left(H^{(n,m)\alpha\beta\chi\delta}\, {}_0\overset{(m)}{E}_{\chi\delta} \right) - {}^{2}_{0}\overset{(n)}{L}{}^{\alpha\beta}_{th} \right\} \right] {}^{0}d\Omega + 2 \int_{{}_0\Omega} \delta\, {}_0\overset{(0)}{E}_{\varsigma 3} \left\{ {}^{1}_{0}\overset{(0)}{L}{}^{\varsigma 3}_{mech} + 2\,\Xi^{(0,0)\varsigma 3\eta 3}\, {}_0\overset{(0)}{E}_{\eta 3} \right\} {}^{0}d\Omega, \qquad \text{(C.1)} $$

where $H^{(n,m)\alpha\beta\chi\delta}$ and $\Xi^{(0,0)\varsigma 3\eta 3}$ are the appropriate parts of the matrix $\left[{}_0\mathcal{H}_{mech} \right]$ (B.12).

The strain increments are obtained ([12, 57]) from

$$ {}_0E_{ij} = \frac{\partial {}^{1}_{0}E_{ij}}{\partial q_S} \Delta q_S \,, \qquad \text{(C.2)} $$

whereas their variations come out ([12, 57]) from

$$ \delta({}_0E_{ij}) \cong \frac{\partial {}^{1}_{0}E_{ij}}{\partial q_S} \delta q_S + \frac{\partial^2 {}^{1}_{0}E_{ij}}{\partial q_S \partial q_T} \delta q_S \Delta q_T \,, \qquad \text{(C.3)} $$

where q_i are the nodal displacements of finite elements.

Substitution of (C.2) and (C.3) into (C.1) leads to the following form of the internal virtual work

$$ {}^{2}\delta W_i = \delta q_S \left\{ {}^{1}_{0}F_S - {}^{2}_{0}F^{th}_S + \left({}^{1}_{0}K^{U}_{ST} + {}^{1}_{0}K^{G}_{ST} - {}^{2}_{0}K^{G,th}_{ST} \right) \Delta q_T + \underbrace{ {}^{1}_{0}K^{U(II)}_{STR} \Delta q_T \Delta q_R }_{J_S({}^{1}q, \Delta q)} \right\}, \qquad \text{(C.4)} $$

where:

${}^{1}_{0}F_S$ - represents the components of the balanced force vector ${}^{1}_{0}\mathbf{F}$ in the actual (t=1) configuration:

$$ {}^{1}_{0}F_S = \int_{{}_0\Omega} \left[\sum_{n=0}^{2} \frac{\partial\, {}^{1}_{0}\overset{(n)}{E}_{\alpha\beta}}{\partial q_S}\, {}^{1}_{0}\overset{(n)}{L}{}^{\alpha\beta}_{mech} + 2 \frac{\partial\, {}^{1}_{0}\overset{(0)}{E}_{\varsigma 3}}{\partial q_S}\, {}^{1}_{0}\overset{(0)}{L}{}^{\varsigma 3}_{mech} \right] {}^{0}d\Omega, \qquad \text{(C.5)} $$

${}^{2}_{0}F^{th}_S$ - symbolizes the components of the thermal load vector ${}^{2}_{0}\mathbf{F}_{th}$, which depend on the actual (t=1) displacements and temperature in the unknown (t=2) configuration:

$$ {}^{2}_{0}F^{th}_S = \int_{{}_0\Omega} \left[\sum_{n=0}^{2} \frac{\partial\, {}^{1}_{0}\overset{(n)}{E}_{\alpha\beta}}{\partial q_S}\, {}^{2}_{0}\overset{(n)}{L}{}^{\alpha\beta}_{th} \right] {}^{0}d\Omega, \qquad \text{(C.6)} $$

${}^{1}_{0}K^{U}_{ST}$ - stands for the components of the constitutive matrix ${}^{1}_{0}\mathbf{K}_U$ dependent on the actual (t=1) displacements:

$$ {}^{1}_{0}K^{U}_{ST} = \int_{{}^{0}\Omega} \left[\sum_{n=0}^{2}\sum_{m=0}^{2} \left(\frac{\partial {}^{1}_{0}E^{(n)}_{\alpha\beta}}{\partial q_S} H^{(n,m)}_{\alpha\beta\chi\delta} \frac{\partial {}^{1}_{0}E^{(m)}_{\chi\delta}}{\partial q_T} \right) + 4 \frac{\partial {}^{1}_{0}E^{(0)}_{\zeta 3}}{\partial q_S} \Xi^{(0,0)}_{\zeta 3 \eta 3} \frac{\partial {}^{1}_{0}E^{(0)}_{\eta 3}}{\partial q_T} \right] {}^{0}d\Omega, \tag{C.7} $$

${}^{1}_{0}K^{G}_{ST}$ - denotes the components of the geometric stiffness matrix ${}^{1}_{0}\mathbf{K}_{G}$ dependent on the actual (t=1) stresses:

$$ {}^{1}_{0}K^{G}_{ST} = \int_{{}^{0}\Omega} \left[\sum_{n=0}^{2} \frac{\partial^2 {}^{1}_{0}E^{(n)}_{\alpha\beta}}{\partial q_S \partial q_T} {}^{1}_{0}L^{(n)}_{mech\,\alpha\beta} + 2 \frac{\partial^2 {}^{1}_{0}E^{(0)}_{\zeta 3}}{\partial q_S \partial q_T} {}^{1}_{0}L^{(0)}_{mech\,\zeta 3} \right] {}^{0}d\Omega, \tag{C.8} $$

${}^{2}_{0}K^{G,th}_{ST}$ - indicates the components of the thermal stiffness matrix ${}^{2}_{0}\mathbf{K}_{G,th}$ dependent on the temperature in the unknown (t=2) configuration:

$$ {}^{2}_{0}K^{G,th}_{ST} = \int_{{}^{0}\Omega} \left[\sum_{n=0}^{2} \frac{\partial^2 {}^{1}_{0}E^{(n)}_{\alpha\beta}}{\partial q_S \partial q_T} {}^{2}_{0}L^{(n)}_{th\,\alpha\beta} \right] {}^{0}d\Omega, \tag{C.9} $$

${}^{1}_{0}K^{U(II)}_{STR}$ - refers to the components of the additional three dimensional object, which is called a higher order matrix and depends on the actual (t=1) displacements [57]:

$$ {}^{1}_{0}K^{U(II)}_{STR} = \int_{{}^{0}\Omega} \left[\sum_{n=0}^{2}\sum_{m=0}^{2} \left(\frac{\partial^2 {}^{1}_{0}E^{(n)}_{\alpha\beta}}{\partial q_S \partial q_R} H^{(n,m)}_{\alpha\beta\chi\delta} \frac{\partial {}^{1}_{0}E^{(m)}_{\chi\delta}}{\partial q_T} \right) + 4 \frac{\partial^2 {}^{1}_{0}E^{(0)}_{\zeta 3}}{\partial q_S \partial q_R} \Xi^{(0,0)}_{\zeta 3 \eta 3} \frac{\partial {}^{1}_{0}E^{(0)}_{\eta 3}}{\partial q_T} \right] {}^{0}d\Omega. \tag{C.10} $$

In the matrix notation, the internal virtual work (C.4) can be expressed as follows

$$ {}^{2}\delta W_i = \delta \mathbf{q}^T \left({}^{1}_{0}\mathbf{F} - {}^{2}_{0}\mathbf{F}_{th} + \left({}^{1}_{0}\mathbf{K}_{U} + {}^{1}_{0}\mathbf{K}_{G} - {}^{2}_{0}\mathbf{K}_{G,th} \right) \Delta \mathbf{q} + \mathbf{J}\left({}^{1}\mathbf{q}, \Delta \mathbf{q} \right) \right) \tag{C.11} $$

what consequently leads to the incremental equilibrium equation:

$$ \left({}^{1}_{0}\mathbf{K}_{U} + {}^{1}_{0}\mathbf{K}_{G} - {}^{2}_{0}\mathbf{K}_{G,th} \right) \Delta \mathbf{q} = {}^{2}_{0}\mathbf{F}_{th} - {}^{1}_{0}\mathbf{F} - \left\{ \mathbf{J}\left({}^{1}\mathbf{q}, \Delta \mathbf{q} \right) \right\} \tag{C.12} $$

One has to notice, that the vector $\mathbf{J}\left({}^{1}\mathbf{q}, \Delta \mathbf{q} \right)$ present in (C.12), as being non-linear with respect to the displacement increment, is omitted in the linearized form of incremental equilibrium equation:

$$ \left({}^{1}_{0}\mathbf{K}_{U} + {}^{1}_{0}\mathbf{K}_{G} - {}^{2}_{0}\mathbf{K}_{G,th} \right) \Delta \mathbf{q} = {}^{2}_{0}\mathbf{F}_{th} - {}^{1}_{0}\mathbf{F} \,. \tag{C.13} $$